MARKER STUDIES

of

NICKEL SILICIDE FORMATION

by

JOHN EDWARD McLEOD

Dissertation presented to the
University of Cape Town
in fulfilment of the requirements
for the degree of

MASTER OF SCIENCE

Department of Physics
University of Cape Town

April 1988

ABSTRACT

Atomic diffusion during the solid state formation of thin films of nickel silicides (Ni_2Si and NiSi) from nickel and amorphous silicon has been investigated using ^{31}Si radioactive tracer and inert marker techniques. Samples were prepared by vacuum deposition of thin films of nickel and silicon, followed by thermal annealing to effect silicide growth.

The radioactive tracer investigation of Ni_2Si showed nickel to be the diffusing species during silicide growth. Sharply defined Ni_2Si^* profiles of 100% radioactive concentration at the sample surface were obtained. The results are compared with previous results in which the profiles were more spread out and of lower surface concentration.

The radioactive tracer investigation of NiSi formation showed that nickel is also the diffusing species during second phase growth. The $NiSi^*$ layer was found to be of 100% concentration. Some spreading of the activity profile near the $NiSi/NiSi^*$ interface was observed. The results were consistent with previous ^{31}Si tracer work on NiSi formation and also with the present Ni_2Si^* results.

The inert marker investigation used an ultra-thin (5-10 Å) continuous layer of Mo or Ta to monitor atomic movement during silicide growth. The results confirmed nickel to be the diffusing species during the growth of both phases. These results are in excellent agreement with previous inert marker studies of nickel silicide growth.

ACKNOWLEDGEMENTS

This work would not have been possible without the help of a number of people. I would like to express my appreciation to the following:-

My supervisor, Dr. C.M. Comrie, Physics Dept. Univ. of Cape Town, for his guidance, participation, and supervision of this investigation, for expert tuition in practical experimental techniques, and for his enthusiasm and friendship.

My external supervisor, Dr R. Pretorius, Ion-solid Interaction Division, National Accelerator Centre, for his guidance, participation, and supervision of this work, for sharing his expertise in the field of study, and for support and friendship.

Dr. D. Reitmann, Director of the National Accelerator Centre, and Dr. W.R. McMurray, Head of the Van der Graaf Group, for financial support and for the use of the facilities at NAC.

The Foundation for Research and Development, CSIR, for financial support.

Mr P. Groenewald, for his expert help with the preparation of diagrams.

The technical staff of the Van der Graaf Group, NAC, for their friendly assistance and efficient maintenance of equipment, and for their ready co-operation in providing accelerator beam facilities at any hour of the day or night.

Dr. M.A.E. Wandt, Ion-solid Interaction Division, NAC, and Dr. C.M. Comrie, for helping with the tedious all-night tracer experiments.

My family for their moral and financial support.

And finally, my friends and associates at NAC and UCT, for their encouragement and friendship.

CONTENTS

CHAPTER 1

INTRODUCTION AND BACKGROUND THEORY

1.1 INTRODUCTION

Silicon forms compounds of the form M_xSi_y, known as silicides, with most of the metals. Many of these, particularly those of the transition elements, are high stability compounds with metallic character, and as such are extensively used in solid state devices. Table 1.1 gives a listing of the currently known transition metal silicides; it can be seen that the list is extensive.

Silicides may be prepared by a variety of techniques; e.g. bulk heating of metal with silicon, co-deposition of metal and silicon by sputter, chemical vapour, or vacuum deposition methods, or thin film metal deposition followed by thermal or laser annealing. During this investigation silicides were prepared exclusively by vacuum evaporation of thin metal films followed by furnace annealing at low temperatures, thus producing thin film silicides by solid state reaction. This method is widely used in device preparation due to its compatibility with other fabrication processes.

Thin film silicides have essentially the same properties as bulk silicides, but when grown in this manner, in the presence of excess silicon, many of the phases do not

Table 1.1

Silicides Formed by the Transition Metals and Group IB and IIB Metals. (Ref. 1).

Group IIIB	Group IVB	Group VB	Group VIB	Group VIIB	Group VIII			Group IB	Group IIB
Sc	Ti	V	Cr	Mn	Fe	Co	Ni	Cu	Zn
Sc_5Si_3	Ti_3Si	V_3Si	Cr_3Si	Mn_6Si	Fe_3Si	Co_3Si	Ni_3Si	Cu_5Si	
ScSi	Ti_5Si_3	V_2Si	Cr_2Si	Mn_9Si_2	Fe_5Si_3	Co_2Si	Ni_5Si_2	Cu_4Si	
Sc_2Si_3	Ti_5Si_4	V_5Si_3	Cr_5Si_3	Mn_3Si	FeSi	CoSi	Ni_2Si	$Cu_{15}Si_4$	
Sc_3Si_5	TiSi	V_5Si_4	Cr_3Si_2	Mn_5Si_2	$FeSi_2$	$CoSi_2$	Ni_3Si_2	Cu_3Si	
	$TiSi_2$	VSi_2	CrSi	Mn_5Si_3		$CoSi_3$	NiSi	CuSi	
			$CrSi_2$	MnSi			$NiSi_2$		
				Mn_3Si_5					
				$Mn_{11}Si_{19}$					
				Mn_4Si_7					
				$MnSi_2$					
Y	Zr	Nb	Mo	Tc	Ru	Rh	Pd	Ag	Cd
Y_5Si_3	Zr_4Si	Nb_4Si	Mo_3Si		Ru_2Si	Rh_2Si	Pd_5Si		
Y_5Si_4	Zr_3Si	Nb_3Si	Mo_5Si_3		Ru_3Si_2	Rh_5Si_3	Pd_9Si_2		
YSi	Zr_2Si	Nb_2Si	Mo_3Si_2		RuSi	$Rh_{30}Si_{13}$	Pd_4Si		
Y_3Si_5	Zr_5Si_3	Nb_5Si_3	$MoSi_2$		Ru_2Si_3	Rh_3Si_2	Pd_3Si		
$YSi_{1,7}$	Zr_3Si_2	$NbSi_2$				$Rh_{58}Si_{42}$	Pd_9Si_4		
YSi_2	Zr_4Si_3					RhSi	Pd_2Si		
	Zr_5Si_4					Rh_4Si_5	PdSi		
	Zr_6Si_5					Rh_3Si_4			
	ZrSi					Rh_2Si_3			
	$ZrSi_2$					$RhSi_2$			
La	Hf	Ta	W	Re	Os	Ir	Pt	Au	Hg
La_5Si_3	Hf_2Si	$Ta_{4,5}Si$	W_5Si_3	Re_3Si	OsSi	Ir_3Si	Pt_4Si		
La_3Si_2	Hf_5Si_3	Ta_4Si	W_5Si_3	Re_5Si_3	Os_2Si_3	Ir_2Si	Pt_3Si		
LaSi	Hf_3Si_2	Ta_3Si	W_3Si_2	ReSi	$OsSi_{1,8}$	Ir_3Si_2	Pt_5Si_2		
$LaSi_2$	Hf_4Si_3	Ta_2Si	WSi_2	$ReSi_2$	$OsSi_2$	IrSi	$Pt_{12}Si_5$		
	Hf_5Si_4	Ta_5Si_3			$OsSi_3$	Ir_2Si_3	Pt_7Si_3		
	HfSi	$TaSi_2$				$IrSi_{1,75}$	Pt_2Si		
	$HfSi_2$					$IrSi_2$	Pt_6Si_5		
						$IrSi_3$	PtSi		

appear; e.g. for nickel, only the dimetal silicide Ni_2Si, the monosilicide NiSi, and the disilicide $NiSi_2$ are evident.

Furthermore it is normally the most silicon rich silicide which is thermodynamically stable in the presence of excess silicon. Only a small subset of the silicides listed in table 1.1 are consequently suitable for use in solid state devices. Table 1.2 lists some of these silicides together with their lowest binary eutectic temperature and specific resistivity. For comparison purposes Table 1.3 gives similar information for the corresponding metals.

Table 1.2 Lowest Eutectic Temperatures and Resistivities of Some Silicides of Interest (Ref. 2).

Silicide	Lowest Binary Eutectic Temp. °C	Specific Resistivity ($\mu\Omega$-cm)
$CoSi_2$	1195	18-25
$HfSi_2$	1300	45-50
$MoSi_2$	1410	100
$NbSi_2$	1295	50
$NiSi_2$	966	50-60
Pd_2Si	720	30-35
PtSi	830	28-35
$TaSi_2$	1385	35-45
$TiSi_2$	1330	13-25
VSi_2	1385	50-55
WSi_2	1440	70
$ZrSi_2$	1355	35-40

Silicides are used as contacts, both ohmic and rectifying, and as gate and interconnection metallization in solid state devices. A brief description of these uses is given in the following section.

Table 1.3 Melting points and Resistivities for Refractory Metals of Interest (Ref. 2).

Metal	Melting Point °C	Specific Resistivity (μΩ-cm)
Co	1497	9,8
Hf	2226	35
Mo	2615	5,7
Nb	2472	12
Ni	1455	7,8
Pd	1554	11
Pt	1772	10
Ta	2996	15,5
Ti	1670	41
V	1903	25
W	3417	5,6
Zr	1855	41

1.2 SILICIDES AND SOLID STATE DEVICES

Integrated circuit (IC) fabrication processes can produce structures with the required electrical characteristics. To utilize the devices, electrical connections i.e., contacts, must be made to various parts of the structure. Because it has been found impracticable to attach wires directly to silicon an intervening conducting film, usually metallic, is employed. Figures 1.1 and 1.2 show this contact metallization schematically for an NPN junction IC transistor and a typical MOSFET, respectively.

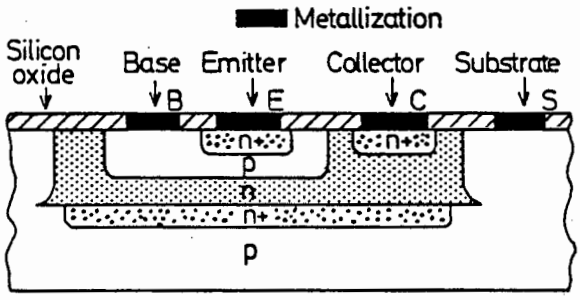

Figure 1.1 Schematic of a buried collector NPN IC bipolar junction transistor showing contact metallization. (Ref. 3).

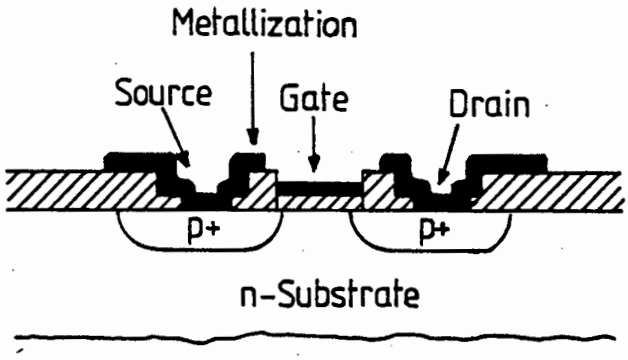

Figure 1.2 Contact and gate metallization in a typical MOSFET. (Ref. 4).

The requirements for the metallization layer are stringent. Apart from the obvious properties of low resistivity and high stability, it must make good ohmic (non-rectifying) contact with the silicon, have suitable metallurgical properties for lead attachment or form good contact with the final metallization overlayer, and maintain its metallurgical integrity during the high temperatures required for IC fabrication.

Many different metals e.g. gold, aluminium, lead, silver, chromium, and palladium, have been used for this purpose. For various reasons[5] none of these is ideal, but Al is most commonly used. Recently attention has been directed toward the use of refractory metal silicides, such as $MoSi_2$, WSi_2, $TiSi_2$, and $TaSi_2$, for ohmic contacts.[6] They are of relatively low electrical resistivity, can withstand the chemical reagents, oxidizing atmospheres and high temperatures encountered during device manufacture, and have the additional

advantage that they can be covered with their own thermally grown SiO_2 layer for protection or insulation.

When a metal makes contact with a semiconductor the Fermi levels match up. Due to the differing work functions of the metal and semiconductor a potential barrier to charge transfer, known as the Schottky barrier, results. Such a barrier is rectifying if the work function of the metal is greater than that of the semiconductor. Ohmic contacts are approximated in practice if the semiconductor is heavily doped. Typically structures such as metal-n^+-n or metal-p^+-p, (where the $^+$ indicates heavy doping, ~ $\geq 10^{19}$ atoms/cm^3), which are really low or degenerate barriers, are constructed as ohmic contacts.

Rectifying Schottky contacts, called Schottky diodes, have some attractive and useful features. The diode operates as a majority carrier device, eliminating storage time due to minority carrier storage, and hence giving an inherently fast response time. Also the forward turn-on voltage is lower than for a diffused junction so that the Schottky diode can be used as a clamp to prevent transistors going deeply into saturation. Schottky diodes are consequently widely used in integrated circuits; as for instance in the Schottky TTL logic family.[7]

Silicides are extensively used in Schottky diodes. The silicides are formed by solid state reaction between the metal film and the silicon. This results in the

silicon/silicide interface being free of surface imperfection or contamination so that reliable and reproducible barriers are produced. Barrier heights, which control the contact properties, vary from 0,55 eV for $ZrSi_2$ to 0,94 eV for $IrSi_3$. PtSi, with barrier height of 0,87 eV, is most frequently used.[2]

The trend in the micro-electronics industry has always been toward greater packing density of elements, and with the advent of VLSI (very large scale integration), Al has presented problems as the gate and interconnection metallization material. Smaller structures have necessitated thinner (possibly sub-micron) interconnection lines, resulting in higher current densities. Excessively high current densities (e.g. ~ 10^5 A/cm² in Al and 10^6 A/cm² in Au) produce the phenomenon of electromigration, the mass transport of metal atoms by momentum exchange with the conducting electrons. The metal disappears from certain regions and accumulates in others, until ultimately an open or short circuit occurs, and the device fails.

Contact alloying is used to form good contact between the metal and semiconductor in ohmic contacts. The Al/Si structure is heated (at temperatures below the Si/Al eutectic of 577 °C) resulting in the silicon diffusing into the Al. Uneven dissolution of the silicon results in voids which eventually become backfilled with Al to form conducting spikes. This is not significant if the junction

is deep enough, but VLSI technology has necessitated the use of shallow junction devices, resulting in possible leaky or shorted junctions (Fig. 1.3).

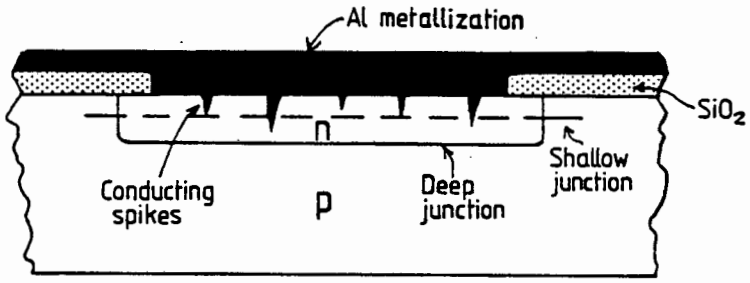

Figure 1.3 Conducting spikes resulting from contact alloying with aluminium metallization. The spikes can cause device failure in shallow junction VLSI devices.

VLSI structures have thus required alternative metallization materials. Polysilicon has been widely used, but it has the disadvantage of having a high specific resistivity (>300$\mu\Omega/cm^2$ even when highly doped) leading to slower and less efficient devices. Silicides, with their intermediate value of specific resistance, are an attractive material for use in this context. Of the silicides PtSi is the most widely used. When grown by solid state reaction from a thin Pt film growth is laterally uniform, eliminating alloy spiking effects. Also silicides have high melting points and are thus expected to have high electromigration resistance.[8]

Since silicides are most frequently produced by solid state reactions, considerable research in recent years has been directed towards understanding these rather complex reactions. In the following sections some of the factors and

theories applicable to silicon/thin-metal-film solid state reactions, Si/Ni in particular, are discussed.

1.3 SILICIDE GROWTH KINETICS

The growth of thin film silicides by thermal annealing has been found to occur by one of two distinct kinetic patterns; viz. formation of laterally uniform silicide layers with well-defined kinetics and temperature dependence, or rapid, non-uniform growth with critical temperature dependence.

Most of the di- and mono- transition metal silicides fall within the former group. Growth occurs over a fairly wide temperature range with rate depending exponentially upon temperature. Growth rate may follow a $t^{1/2}$ time dependence, indicating a diffusion controlled reaction, or be linear with time if the rate limiting step is the interfacial reaction. Typical examples are Ni_2Si, NiSi, Co_2Si, CoSi, Pd_2Si, Pt_2Si, and PtSi, which form by diffusion controlled reactions, and $TaSi_2$ and $CrSi_2$ formation which occur by interface controlled reactions.[5,9]

It is of practical importance to measure the rate constants and activation energies of these reactions. For a diffusion controlled reaction we have

$$x = kt^{1/2} \tag{1.1}$$

and for an interface controlled reaction

$$x = kt \tag{1.2}$$

where x is the silicide thickness grown at time t, and k is

the rate constant. Since the silicide grows in well-defined layers with sharp interfaces, thickness measurement is relatively straightforward, and can be accomplished with analytic techniques such as RBS, TEM, and optical or X-ray spectroscopy. The temperature dependence of k is given by

$$k = k_o \exp(-E_a/k_b T) \qquad (1.3)$$

where k_b is Boltzmans constant, T is absolute temperature, and E_a the activation energy. An Arrhenius plot (ln k vs. 1/T) is subsequently used to determine E_a.

Considerable effort has already been made to determine these parameters. Reproducibility and consistency are, however, not good since the reactions are extremely sensitive to uncontrollable factors, such as impurity content and structure of the metal or silicon. Comprehensive data on silicide growth kinetics may be found in Ref. 9.

The growth kinetics of silicides which form in a laterally non-uniform manner are less amenable to simple analysis. Growth begins at nucleation centers, then proceeds rapidly in all directions, producing a non-uniform layer. Interfaces are less well-defined and extent of reaction (i.e. silicide thickness) is difficult to asses.

Nucleation controlled reactions only proceed above a certain critical temperature. The reaction, $NiSi + Si_{<100>} \rightarrow NiSi_2$, is an example, with reaction only occurring above about 750°C.[32] Various reasons for the existence of the critical

temperature (e.g. kinetic or thermodynamic) have been postulated but a definitive explanation is still awaited.

1.4 EFFECT OF IMPURITIES

Solid state reactions are highly sensitive to impurity contamination. The specific effect depends upon the impurity and its concentration, but generally the reaction rate is reduced or the reaction is completely inhibited. In silicide formation by thermal annealing the sequential order of phase appearance may be completely altered; certain phases may not appear or structures with multiple phases may grow.

In thin film structures formed by vacuum evaporation impurities are inevitably present, both as interfacial layers, and in distributed form throughout the layers. Oxygen bonds very strongly to silicon (ΔH_f^{SiO2} = -217,6 kcal/mol)[12] and also forms stable oxides with the transition metals (e.g. ΔH_f^{NiO} = -57,5 kcal/mol)[12] so that during evaporation in the necessarily imperfect vacuum incorporation of oxides is inevitable. Oxygen and nitrogen also diffuse into the upper layer of the samples during annealing and during transfer from evaporating chamber to annealing furnace. Furthermore after sample cleaning the samples are exposed to air prior to loading into the evaporation chamber, resulting in the growth of a layer of SiO_2, commonly called, 'the native oxide layer'.

The effect of distributed impurities has been shown[10] to depend on the initial distribution and on the diffusing species during the reaction. This is shown schematically in Fig. 1.4 for first phase (M_2Si) formation.

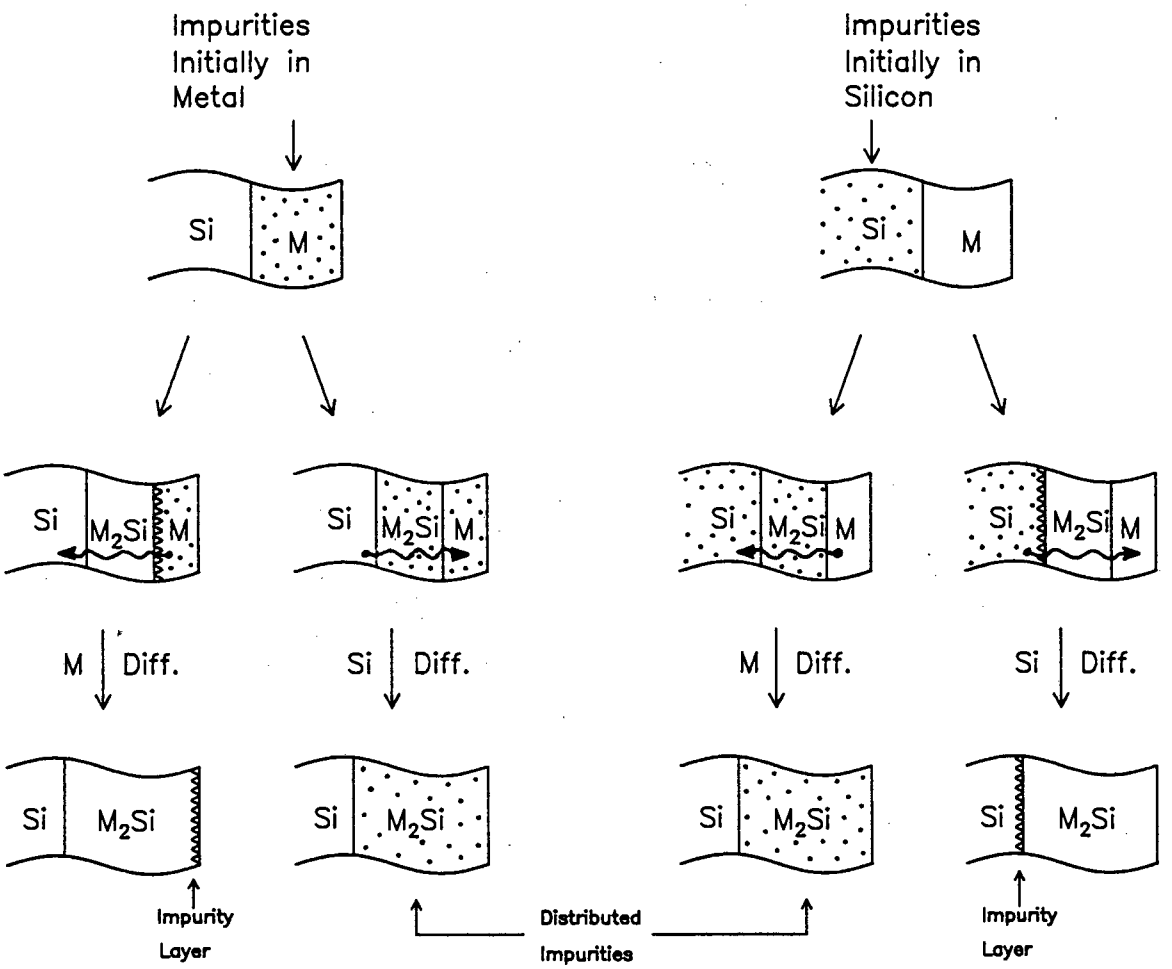

Figure 1.4 Impurity redistribution during silicide growth. Final location and distribution of impurities depends on the initial distribution and the diffusing species during reaction.

If silicon is the diffusing species, impurities initially within the metal remain distributed throughout the silicide, and similarly for M diffusion when the impurities are initially in the silicon. However when the impurities are

initially within the layer which provides the diffusing species, the impurities are left behind and an interfacial layer results. The argument is readily extended to subsequent phase formation.

The specific effect of many different impurities in silicide reactions have been widely researched by deliberately introducing the impurities into the structure prior to growth. Details of these investigations may be found in the literature. Ref. 5 discusses some of the results while ref. 11 includes a comprehensive literature survey of the effects of impurities on silicide growth.

1.5 PHASE FORMATION AND REACTION THERMODYNAMICS

It is evident from Table 1.1 that metal-silicon compounds form many phases with varying Si/M content. In general the number of phases which form varies from one to about ten. The existence of these phases are known from experimental observations. It has not proved possible to reliably predict the formation of specific phases in a given silicide in terms of the fundamental properties (atomic, molecular, crystal, chemical etc.) of the element concerned. Attention has thus been directed rather towards examination and explanation of the observed phase formation, (first phase, subsequent phases, stability of phases etc.) in the light of experimentally derived information, such as binary phase diagrams, and thermodynamic and kinetic data for the reaction.

Thermodynamic Aspects

In solid state reactions entropy change is generally small and ΔH_f, the formation enthalpy, is usually used to approximate ΔG_f , the Gibbs energy of formation. ΔH_f has been determined for a large number of silicides[5,9] and is generally about -20 to -30 kcal/mol. In all cases ΔH_f is negative so that the formation of silicides is thermodynamically favorable. For thin film silicide reactions the number of metal atoms is fixed and limited, so that ΔH_f per metal atom is representative of the total energy gain after formation of a particular phase. As pointed out by Murarka[5] the energy gain/metal atom generally increases with silicon content, so it is expected, and observed, that the most stable phase is the most silicon rich one.

The observed phase sequence for nickel (in the presence of excess silicon) together with thermodynamic data is given in Fig. 1.5. The first two phases have relatively large ΔH_f to act as driving force and reactions are diffusion limited and occur at relatively low temperatures. Third phase, $NiSi_2$, has however very low ΔH_R (from NiSi), and the reaction only proceeds at higher temperatures (ca. $\geq$ 750 °C), perhaps as a result of a favorable $T\Delta S$ term ($\Delta S_R^{298}{}_{NiSi+Si \rightarrow NiSi2}$ = +5 cal/deg mol)[12], becoming significant. On thermodynamic grounds it may thus be argued that if $-\Delta H_f$ for third phase formation could be increased the reaction should occur at lower

temperature. This is indeed observed; the reaction of NiSi with amorphous silicon has been reported[45] to take place at about 400 °C. Amorphous silicon is in a higher energy state than crystalline silicon (ΔH_c^{Si} = -2,85 kcal/mol)[13], which significantly increases $-\Delta H_f$ for the reaction.

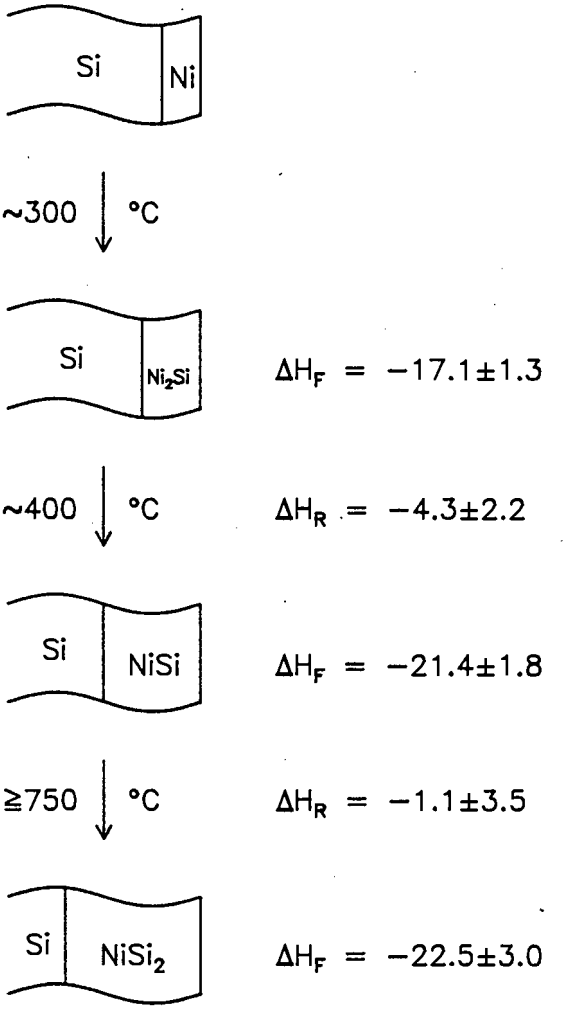

Figure 1.5 Observed phase sequence for the Ni/Si thin film binary diffusion couple upon thermal annealing in the presence of excess Si. ΔH values are given in kcal/mole of Ni, at 298 K. Corrections, $\Delta' H$, (up to the temperatures of reaction), are small. (Ref. 12).

Phase Sequence

The binary phase diagram of an element and silicon contains an enormous amount of (experimentally derived) information on compounds that may form, and their melting temperatures. It thus shows all possible phases that can be formed for a

given metal/silicon system. The phase diagram for Ni/Si is shown in Fig. 1.6, with the different phases, ranging from the most metal rich Ni_3Si, to the most silicon rich $NiSi_2$, indicated.

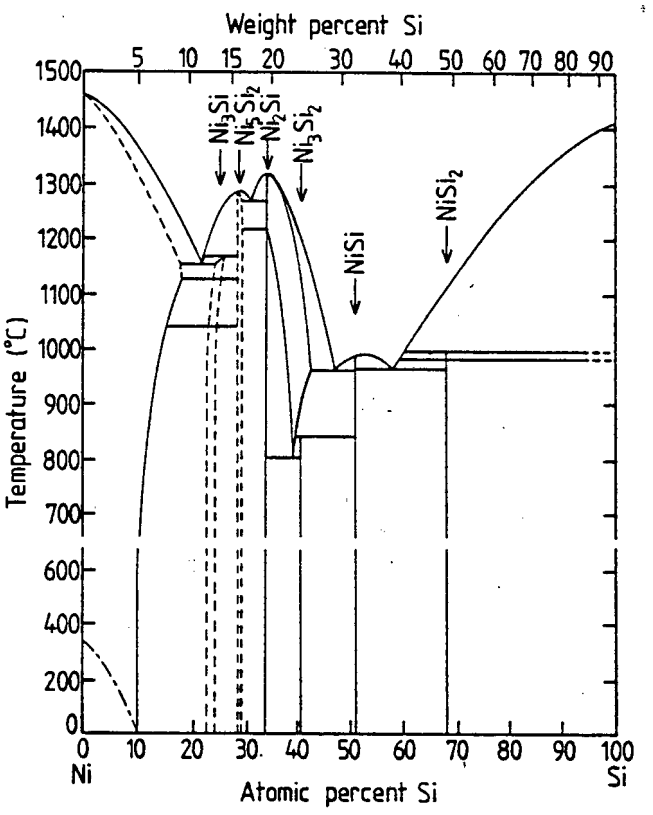

Figure 1.6 Binary phase diagram for the Ni/Si system. The different silicide phases are indicated. (Ref. 14).

A number of methods have been proposed for predicting the sequence of phase formation from these diagrams. The most well known for first phase formation is that due to Walser and Bené[15], who postulated that the metal/silicon interface consists of a metallic glass of concentration near the lowest temperature eutectic, leading to the rule:

> 'The first compound nucleated is the most stable congruently melting compound adjacent to the lowest temperature eutectic.'

Applying this to the Ni/Si diagram, the lowest eutectic is 964 °C and Ni_2Si is the most stable (highest melting point) congruently melting compound adjacent to this, giving the correct result. Application of the rule does in general successfully predict the observed first phase formed.

Ronay[16] used a different argument; the initial concentration at the interface is assumed to be that of the eutectic closest to the center of the phase diagram (in atomic percent) and subsequently to move to the side which provides the diffusing species for the reaction. The reaction mechanism is thus used to explain *why* a particular phase should form.

Tsauer et al[17] extended the argument of Walser and Bené to second phase formation. They proposed that the second phase is the nearest congruently melting phase in the unreacted element. For nickel this is NiSi, as observed.

Pretorius[18] used a thermodynamic approach to show that the first and subsequent phases can be predicted by assuming that the system will always move to minimize its enthalpy, for a given relative concentration of silicon and metal. The concentrations are assumed to start at that of the lowest eutectic and subsequently to move in the direction of the

unreacted element. The analysis shows that phase formation may be governed to a large extent by reaction thermodynamics.

The role of reaction kinetics in determining the observed phase sequence must also be considered. Gösele and Tu[19] modeled the binary diffusion couples mathematically and showed that nucleation of a particular phase must be accompanied by favorable growth rate for the phase to dominate others and grow to macroscopically observable dimensions. For phases that grow with $t^{1/2}$ kinetics the reaction rate slows with increasing layer thickness, leading to the prediction of eventual multiple simultaneous phase growth. Gösele et al[20] have reported the simultaneous existence of all phases Ni_5Si_2, Ni_2Si, Ni_3Si_2, and NiSi, in thick film diffusion couples.

The effect of reaction kinetics on phase sequence can also be demonstrated by the inclusion of impurities to slow the reaction e.g. Nicolet and Scott[21] showed that oxygen implanted in the nickel caused the simultaneous appearance of Ni_2Si and NiSi, while Nicolet et al[22] showed that nitrogen implanted nickel reacts sufficiently slowly to prevent the appearance of Ni_2Si altogether.

1.6 DIFFUSION

Diffusion is an integral part of a solid state reaction and a proper description of the reaction should include a description of the diffusion mechanism and identify the dominant moving species. The theory of diffusion in solids is well-developed and extensive and is comprehensively dealt with in references 24 and 25. The treatment given here must of necessity be very brief.

Diffusion is described macroscopically by Fick's laws of diffusion. Flux J is given by Fick's first law:

$$J = -D(\partial c/\partial x) \tag{1.4}$$

where D is the diffusion coefficient and $\partial c/\partial x$ is the concentration gradient. D is independent of $\partial c/\partial x$ but not necessarily so of the concentration itself.

From the conservation of matter (or fluxant in general) and Eq. 1.4 it is easily shown[23] that

$$\partial c/\partial t = \partial(D\partial c/\partial x)\partial x \tag{1.5}$$

which is Fick's second law for planar diffusion. If D is constant this becomes

$$\partial c/\partial t = D\partial^2 c/\partial x^2 \tag{1.6}$$

To obtain c(x,t) Eq. 1.5 or 1.6 must be solved for the given boundary conditions. The simplest case is an infinitely thin layer diffusing into an infinite system, in which case one obtains[25]

$$c(x,t) = (\alpha/(2\sqrt{\pi Dt}))\exp(-x^2/(4Dt)) \qquad (1.7)$$

where α is the quantity of diffusant.

If the diffusant is initially within a region of finite size then solutions in the form of error functions result. For example, for diffusion out of a plate of thickness 2h and initial concentration c_0[25]

$$c(x,t) = c_0/2 \left\{ \text{erf}((h+x)/(2\sqrt{Dt})) + \text{erf}((h-x)/(2\sqrt{Dt})) \right\} \qquad .....(1.8)$$

For systems of finite size solutions may be built up by superposition of reflections of the infinite system solutions, or obtained by solving Eq. 1.6 by separation of variables.[25] Both methods yield solutions in the form of an infinite sum of terms.

If D is not constant Eq. 1.5 must be used and solutions in closed form are difficult to obtain. In cases where $D \neq D(c)$ and the initial conditions can be expressed in terms of a single variable $\eta = x/t^{1/2}$ the Boltzman-Matano analysis may be used.[23] Equation 1.5 is transformed into an ordinary homogeneous differential equation and suitable graphical integration of experimental results yields values of D(c).

The application of diffusion theory to phase growth is a non-trivial task. Nevertheless a number of different approaches to the problem have been considered. Kilkaldy[26] has solved Eq. 1.6 (i.e. constant D) for a multi-component

system. For the two component case, his solution reduces to[27]

$$c(x,t) = a + b\ \mathrm{erf}(x/(2\sqrt{Dt})) \qquad (1.9)$$

where the a and b coefficients depend on D and t. However for all but the simplest cases the analysis is too unwieldy to be dealt with practically, and in general the assumption of constant D cannot be justified.

The Matano-Boltzman method[23,28,29] and the analysis due to Kidson[27] examine layer growth without the restriction of constant D. Equation 1.5 is not explicitly solved for c(x,t) but the requirements for layer growth are derived, and the $t^{1/2}$ dependence of layer thickness is shown.

For a better understanding of the diffusion process an atomistic view of diffusion must be considered. In a lattice composed of an ordered matrix of atoms there are two basic diffusion possibilities. The diffusant may move substitutionally by occupying lattice sites, or interstitially by moving through the sub-lattice of vacant interstitial sites between the main matrix atoms. A third possibility is a combination of these two, known as interstitialcy diffusion.

A number of different mechanisms for atom movement substitutionally have been postulated;[24] of these the vacancy mechanism shown in Fig. 1.7 is statistically most probable and (usually) thermodynamically most favoured. The diffusant atoms jump from one lattice site to an adjacent

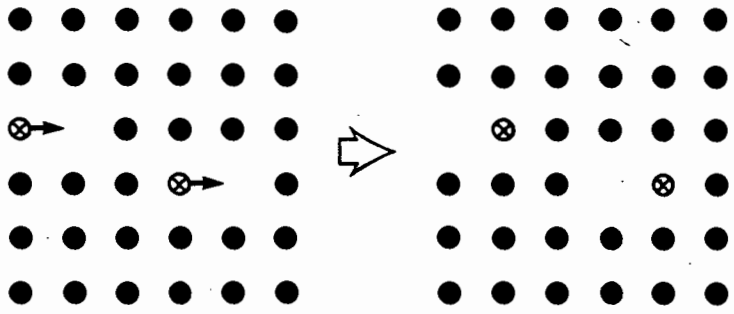

Figure 1.7 Vacancy diffusion. Diffusant moves substitutionally, in opposition to hole movement.

vacant site, so that vacancies and diffusant atoms move in opposite directions. It can be shown[23] that the diffusion coefficient is then proportional to the number of vacancies. Any crystal contains an equilibrium concentration of vacancies N_v^e given by

$$N_v^e = \exp(-\Delta G_v/RT) \qquad (1.10)$$

where ΔG_v is the Gibbs energy required for vacancy creation. As the diffusant moves into the substrate it will fill some of the vacancies so that for this type of diffusion D will be concentration dependant.

Interstitial diffusion is shown in Fig 1.8. Here the diffusant jumps from one interstitial site to another. This type of diffusion is more likely to occur with small diffusant atoms and a relatively open crystal matrix structure. For relatively dilute diffusants the number of unfilled interstitial sites is not significantly altered by the presence of diffusant so that in this case D is more likely to be independent of concentration.

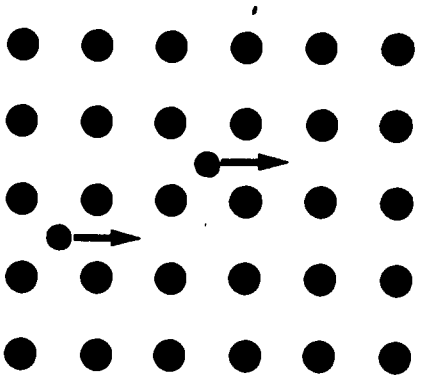

Figure 1.8 Interstitial diffusion. The diffusant atoms move through the lattice without occupying substitutional sites.

For both diffusion mechanisms D is proportional to the jump frequency (ω) with which the diffusant moves from one site to another. For a jump to occur the diffusant atom must move from one low energy position to another, via a high energy intermediate state between sites. The jump frequency may be analyzed in terms of the Gibbs energy (ΔG_a) required to form this high energy state. It is found[23] that

$$\omega = \nu \exp(-\Delta G_a/RT) \qquad (1.11)$$

where ν is the atoms vibrational frequency, usually taken as the Debye frequency.

Equations (1.10) and (1.11) justify the empirically determined form of the temperature dependence of the diffusion coefficient

$$D = D_0 \exp(-Q_a/RT) \qquad (1.12)$$

where Q_a is termed the activation energy for the diffusion process. Equation (1.12) is frequently used to obtain D from experimental results.

When the substrate material is polycrystalline diffusion can also occur along the grain boundaries (GB). In these areas

the substrate atoms are less ordered, ΔG_a is much less, and the jump frequency much higher, leading to rapid diffusion paths. GB diffusion has a low activation energy Q_a so that D is only weakly temperature dependent. Thus GB diffusion is expected to predominate at low temperatures, becoming less significant at higher temperatures.

The mechanism of diffusion in silicide reactions has been widely researched, and much attention has given to the determination of the diffusing species. Marker and tracer techniques used in these studies are discussed in the following sections.

1.7 MARKER TECHNIQUES

The use of inert markers for the study of solid state reactions is well established. The first such marker experiment was performed by Kirkendall and Smigelskas[30], in 1947. Molybdenum wires were used to study the diffusion of copper and zinc in the brass/copper diffusion couple. They were able to show that zinc was the dominant diffusing species.

The basic idea of a marker experiment, as applied to thin film silicide growth, is shown in Fig. 1.9 for first phase (M_2Si), and in Fig. 1.10 for second phase (MSi), silicide growth. In Fig. 1.9 the marker is initially situated at the Si/M interface, and subsequently moves to the surface, or the Si/silicide interface, for M or silicon diffusion,

respectively. In Fig. 1.10 the marker moves from the Si/silicide interface to the center of the second phase silicide for M diffusion, or remains at the interface for silicon diffusion. If both species diffuse, the final marker position depends on the relative diffusion flux of each. Subsequent phase formation is treated similarly to second phase formation.

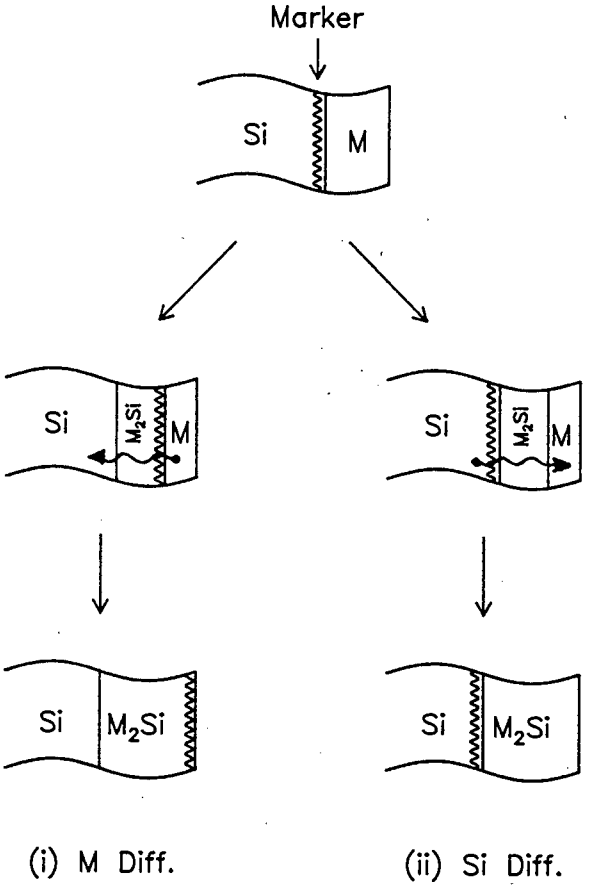

Figure 1.9 Marker experiment on first phase (M_2Si) silicide growth. The marker moves to the surface or the Si/M_2Si interface, depending on the diffusing species.

For thin film silicide reactions markers must of necessity be of microscopic dimensions. Further basic requirements for the markers are (i) that their position within the structure be readily identifiable, both before and after reaction, and

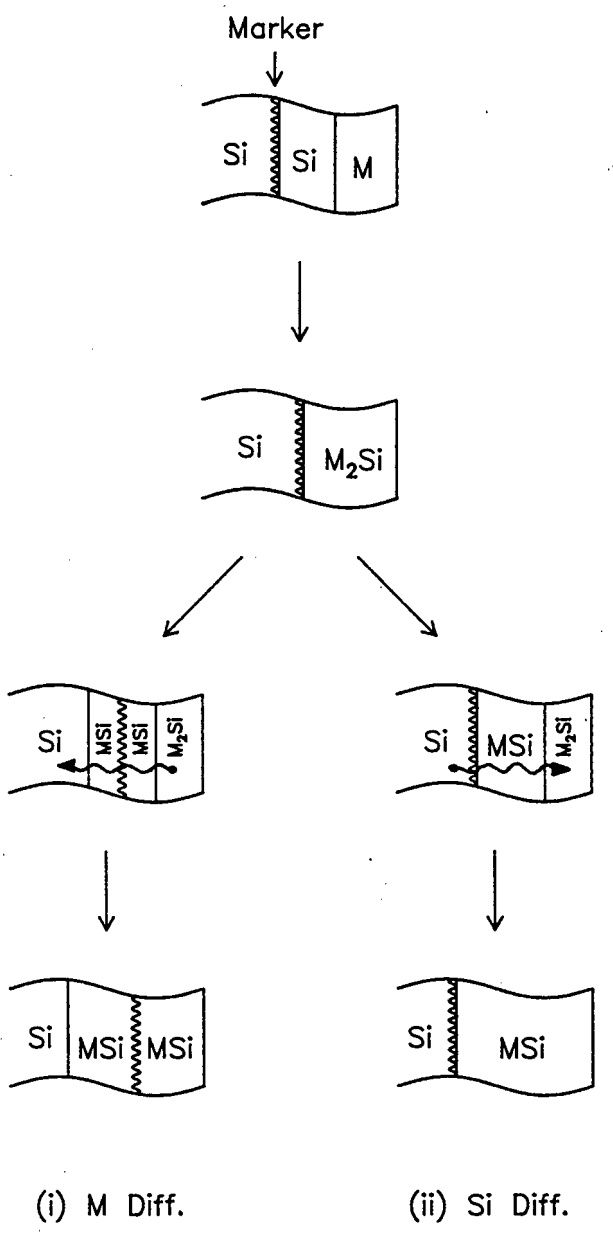

Figure 1.10 Second phase (MSi) marker experiment. The marker moves to the centre of the MSi or to the Si/MSi interface, according to the diffusing species.

(ii) that they do not significantly affect the reaction or its mechanism.

A number of different markers which allegedly satisfy these requirements have been found. Noble gas atoms, Xe, and Ar, positioned by ion implantation, have been extensively used. Thin metal layers, either continuous or partial, (e.g. Pt, W, Ti, and Mo), have also been used. The list of such

experiments is too extensive to treat effectively here. References 9 and 31 contain full listings, and Ref's 9 and 32 discuss marker techniques in more detail.

Nickel silicides have received much attention in marker studies. Table 1.4 lists these experiments and their results. In all cases nickel was found to be the diffusing species. The implications of these results in relation to this work are discussed in the relevant experimental chapters (§ 3.4 & 4.4).

Table 1.4 Nickel Silicide Marker Experiments (Ref. 11).

Silicide	Marker	Diff. Species	Ref.
Ni_2Si	Xe	Ni	34-37
	Ag	Ni	38
	W	Ni	39
NiSi	Xe	Ni	40
	Pt	Ni	41
	^{16}O	Ni	42
$NiSi_2$ (on Si<>)	Xe	Ni	43
	W	Ni	44
$NiSi_2$ (on Si(a))	Xe	Ni	45
	^{18}O	Ni	45

Marker experiments are useful for the study of solid state reactions, but they do have a number of disadvantages:
(i) No inferences can be made about the mechanism of diffusion. The experiments only yield information on the identity of the diffusing species.
(ii) It is difficult to be sure that the presence of the

marker is not, in fact, affecting the reaction. The conclusions reached from a marker experiment may thus not be valid for the reaction without the marker. (iii) The possibility of interface drag[32,33] may lead to erroneous results. If a marker is initially situated at an interface, surface effects may cause it to be dragged along with the interface, irrespective of diffusing species.

To enable further study of silicide reactions suitable radioactive tracer experimental techniques have been developed.

1.8 RADIOACTIVE TRACERS

In a radioactive tracer experiment samples are made with a certain region containing the radioactive isotope. After annealing suitable techniques are used to profile the activity. This allows determination of the diffusing species, and possibly the mechanism of diffusion.

In silicide reactions either the metal or silicon can be used as the radioactive isotope. ^{31}Si has been most widely used in this context; it is easily formed by the reaction $^{30}Si(n,\gamma)^{31}Si$ (cross section 0,1b) and decays with a convenient half-life of 2,62 hours, by emitting β-particles, of maximum energy = 1,48 MeV. Samples may thus be prepared by normal evaporation techniques without harmful or long-lived radioactive contamination of equipment.

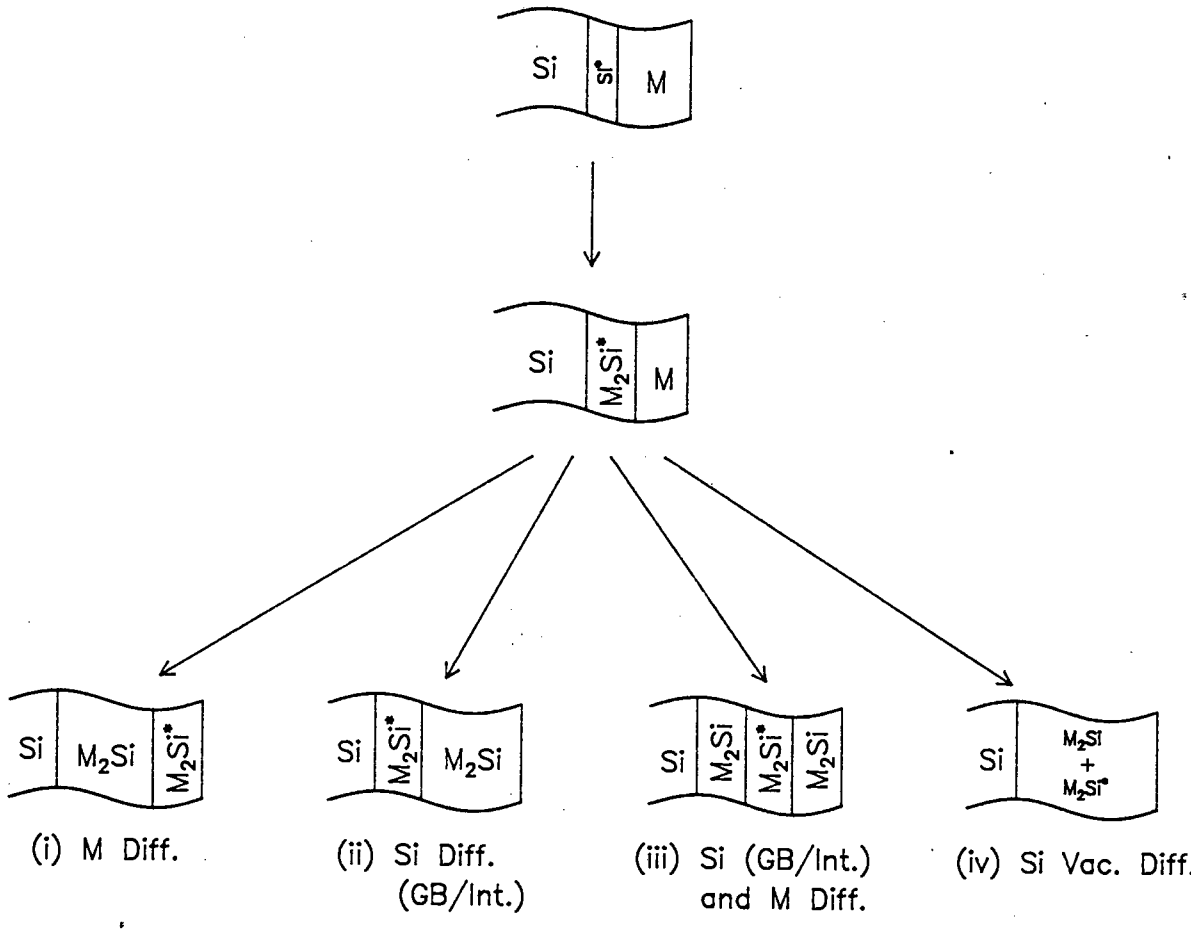

Figure 1.11 First phase (M_2Si) Si^* tracer experimental concept. The M_2Si^* layer moves to the surface for metal diffusion (any mechanism), and to the Si/silicide interface for Si grain boundary (GB) or interstitial (Int.) diffusion. For Si vacancy (Vac.) diffusion spreading of the layer is expected, depending on the degree of exchange between moving Si and fixed Si^* atoms during growth.

Figure 1.11 shows how the ^{31}Si tracer technique is applied to first phase (M_2Si) growth. The final position of the M_2Si^* layer (in (i)-(iii)) depends on the diffusing species and mechanism. If the metal is the diffusing species the Si^* effectively acts as an inert marker, moving to the surface as the metal diffuses through it. No information about the diffusion mechanism can be inferred in this case. If the silicon diffuses through the M_2Si^* layer by interstitial or GB diffusion without exchange with the lattice atoms then

the Si^* again acts as an inert marker, moving to the bottom of the M_2Si layer. The expected profile for silicon vacancy diffusion depends upon the amount of exchange that occurs between the diffusing silicon and the Si^* lattice atoms. If no exchange occurs at all then the silicon just moves straight through the M_2Si^* layer, and the profile of (ii) results. If 100% exchange occurs, i.e. a Si atom moves into the M_2Si^* lattice on one side and a Si^* atom moves out on the other side, then the profile shown in (i) is expected. These assumptions are however rather unrealistic as the random nature of the diffusion process is not taken into account. If an entire macroscopic layer of M_2Si grows by silicon vacancy diffusion then the Si and Si^* atoms must have high mobilities, and considerable mixing of the two is to be expected. Bartur and Nicolet[46], and Lien[47] have analyzed vacancy diffusion in tracer experiments, and have concluded that the mixing would be so thorough as to produce a completely flat profile. This conclusion is supported by flat profiles obtained for $CrSi_2$ and $TiSi_2$ formation (Ref 31), where silicon is known to be the diffusing species[48,34], although it is noted that the flat profiles could have been partly caused by silicon self diffusion at the relatively high annealing temperatures used (490 and 650 °C). Although the actual profile expected for silicon vacancy diffusion is perhaps uncertain, it is assumed, on the basis of the above arguments, that it will not give rise to the profiles of Fig. 1.11 (i) and (ii). It is of course possible for

diffusion during silicide growth to occur by more than one mechanism (see Fig. 1.11). When growth occurs partly by silicon vacancy diffusion then spreading of the profile is expected, the amount of spreading being dependant upon the degree of silicon vacancy diffusion.

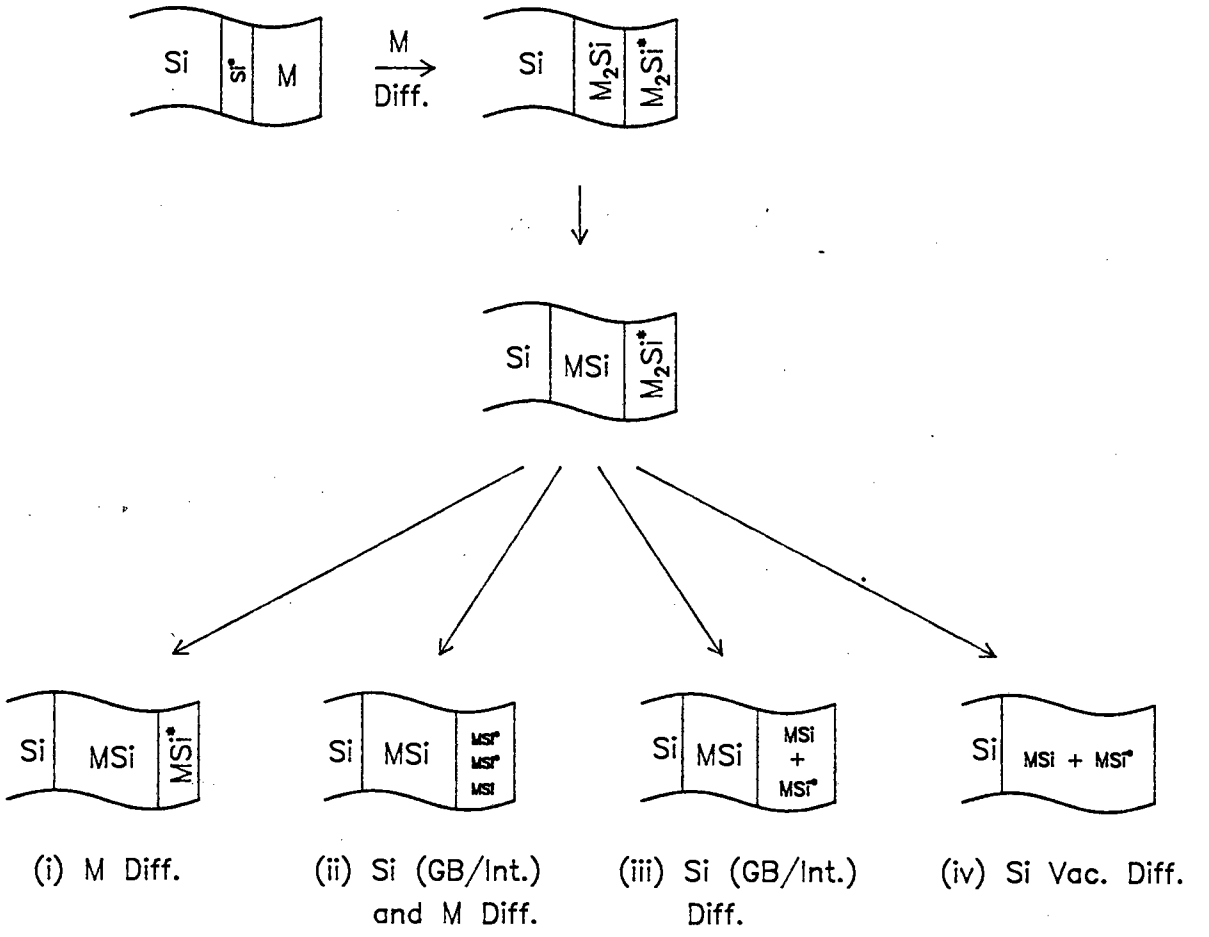

Figure 1.12 Second phase (MSi) Si^* tracer experimental concept (for M diffusion during first phase growth). The Si^* concentration drops to 50% (of that expected for M diff.) if growth occurs by Si (GB or Int.) diffusion. For Si vacancy diffusion the final distribution of the Si^* atoms depends upon the degree of exchange between Si and Si^* atoms during growth.

For second phase investigation a layer of M_2Si^* is first formed within the sample. If the metal is the diffusing

species during first phase growth this layer forms naturally on the surface of the sample (Fig. 1.11 (i)); figure 1.12 shows how the second phase analysis subsequently proceeds. The discussion given above applies equally to this phase, except that in this case it is the radioactive concentration (and hence also the thickness) of the final MSi^* layer which is determined by the diffusion properties. It is again assumed that profiles (i) and (iii) will not result from silicon vacancy diffusion.

Third phase evaluation (where the metal is the diffusing species in the formation of the first two phases) proceeds in a like manner to second phase, starting with the same virgin structure, and ending with a layer of MSi^*_2 ,with radioactive concentration dependant upon diffusion characteristics.

The use of ^{31}Si as a tracer to study solid state reactions was initiated in 1976 by Pretorius et al[49] when the solid phase epitaxy of Si through Pd_2Si was investigated. The technique has since been widely used to investigate a diversity of solid state interactions, such as self diffusion , solid phase epitaxy, and oxidation mechanisms of silicon and silicides. Primary silicide growth has also enjoyed considerable attention, with a number of different silicides and phases being studied. Table 1.5 lists these experiments and their deduced diffusing species.

Table 1.5 ^{31}Si Tracer Experiments on Primary Silicide Growth (Ref. 9).

Silicide	DMS	Ref.
Co_2Si	Co	52
Ni_2Si	Ni	50
Pd_2Si	Pd & Si	51
Pt_2Si	Pt	51
NiSi	Ni	31
PtSi	Pt	54
$TiSi_2$	Si	52
$ZrSi_2$	Si	52
$CrSi_2$	Si	52,53

Radioactive metal marker experiments are less frequently performed as convenient isotopes are not generally to be found. One such tracer experiment was performed by Baglin et al[55] using ^{56}Ni to study nickel silicides, concluding that nickel is the dominant diffusing species in the growth of all three phases. The results of this experiment are considered in greater detail in later chapters (Sections 3.4 & 4.4).

Radioactive tracer experiments have the advantage over inert marker methods in that the tracer atoms are chemically identical to the stable isotopes, and mass effects are expected to be small (~ $(M^{Si31}/M^{Si28})^{½} = (31/28)^{½}$ or ca. 5% for ^{31}Si). Furthermore when the tracer takes part in the diffusion process details concerning the diffusion mechanism can be obtained from the shape of the final activity profile.

Care must however be exercised in the interpretation of results. The tracer profiling technique is subject to large uncertainties so that it is difficult to fit profiles to results with much confidence. The modeling of profiles for the various diffusion mechanisms is also complicated, and results tend to depend, to a large extent, on the assumptions used in the models. Furthermore if the profiles of Fig. 1.11 (i) and Fig. 1.12 (i) are accepted as possibilities for Si vacancy diffusion then, depending upon results, positive identification of the diffusing species may not be possible.[56]

1.9 MOTIVATION AND SCOPE OF THIS INVESTIGATION

Diffusion in nickel silicide reactions has been extensively investigated by inert marker techniques (Table 1.4). The use of ^{31}Si tracer methods to study nickel silicide formation has however been somewhat limited. Ni_2Si formation was studied by Pretorius et al[50]; the results of this work are reproduced here in Fig. 1.13. The method was subsequently applied to NiSi formation from Ni_2Si by Botha[31], but the results were never published. The NiSi results from Botha's work are reproduced here in Fig. 1.14. No attempt has yet been made to apply the technique to $NiSi_2$ formation.

On consideration of Figures 1.13 and 1.14 it is immediately seen that the data in the two experiments appear to be inconsistent with each other. For Ni_2Si formation the radioactive concentration at the surface is shown to have

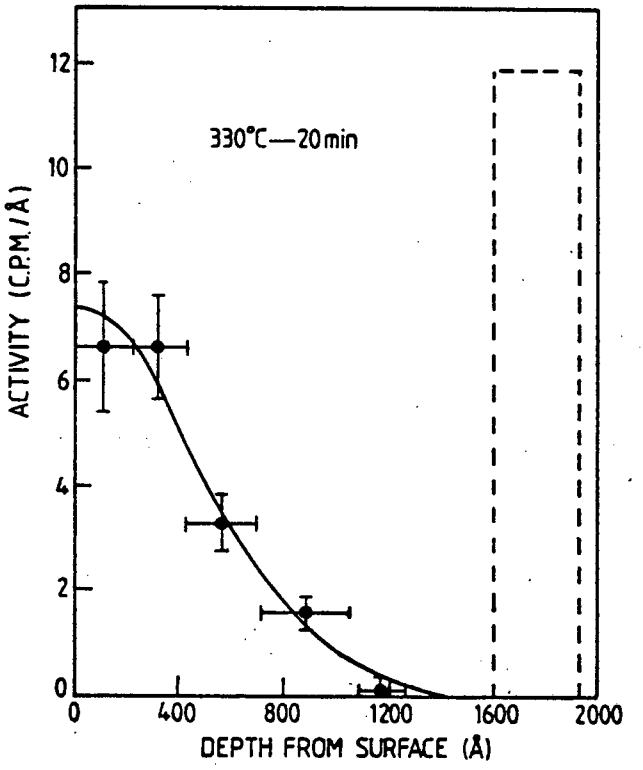

Figure 1.13 Original Ni_2Si ^{31}Si tracer experimental results from Ref. 50. 'Activity profile of the radioactive silicon marker (flagged points) after complete Ni_2Si formation. The radioactive marker profile after initial silicide formation at the Si<100> interface is also shown.'

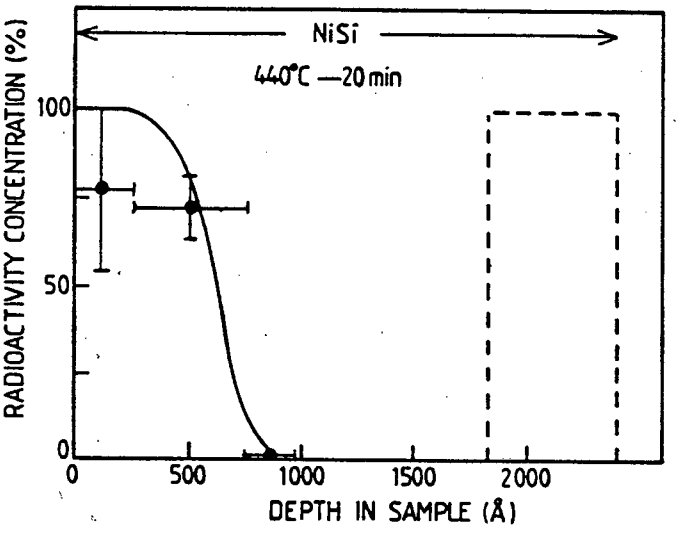

Figure 1.14 Original NiSi ^{31}Si tracer experimental results from Ref.31. 'Radioactive profiles measured after second phase monosilicide formation of NiSi after transformation from Ni_2Si'.

dropped from 12 to about 7,3 cpm/Å, and the profile is considerably broadened. Figure 1.14 however shows 100% activity at the surface, and very little spreading of the Si^*. To perform the NiSi experiment a surface layer of radioactive Ni_2Si is first formed by reaction of nickel with Si^*, following the procedure used in the first phase, Ni_2Si experiment. The inference is thus either that the diffusion mechanism is temperature dependant (ie. different at 440 °C compared to 330 °C), or that during second phase growth the radioactive silicon segregates out into a thin layer, with increased concentration, at the surface. Considering the relatively small temperature differences involved it seems unlikely that the former of these explanations is correct, and the latter action is apparently quite impossible. Furthermore the spreading of the Ni_2Si^* profile shown in Fig. 1.13 tends to imply that the silicon also participated in the diffusion process. Numerous inert marker experiments have however concluded that nickel is the only diffusing species (Table 1.4). The possibility is thus to be considered that the conclusions reached from this earlier work may be questionable.

The growth of $NiSi_2$ from Si<> is not suitable for analysis by ^{31}Si radioactive methods. Growth occurs in a nucleation controlled reaction producing $NiSi_2$ layers with poor lateral uniformity.[32] Furthermore growth only occurs at high temperatures, and rapid spreading of the ^{31}Si due to self diffusion of Si would occur. Botha et al[57] have shown that an initially sharply defined layer of $NiSi^*$ becomes almost

evenly spread throughout the silicide after 20 min. at 750 °C. Lien et al[58] however showed that growth of $NiSi_2$ from NiSi and amorphous silicon occurs at low temperatures (ca. 400 °C) in a diffusion controlled reaction, with good lateral uniformity. Such a reaction should be amenable to analysis by ^{31}Si tracer methods.

On the basis of the above arguments it was decided that further work on nickel silicide formation was justified. The first two phases would be analyzed again, and if possible third phase, $NiSi_2$, growth with amorphous silicon at low temperatures would also be attempted. To support the tracer work it was decided that confirmation of the diffusing species using inert marker experiments was desirable. Since this type of work has been exhaustively applied to nickel silicides already (Table 1.4) it was decided that only minimal effort was warranted, and the simplest type of marker experiment, a thin uniform metal layer as marker, would be performed.

The results of these experiments are presented in the following chapters. The tracer experiments on the first two nickel silicide phases were successful, and are described in chapters 3 (Ni_2Si) and 4 (NiSi). The supplementary inert marker experiments using Pt and Mo as markers on each phase are also discussed in these chapters. Experiments on third phase formation could unfortunately not be attempted as we were unable to obtain consistent uniform growth of $NiSi_2$ at low temperature. Finally chapter 6 summarizes the work and the conclusions that were reached.

CHAPTER 2

EXPERIMENTAL

2.1 SAMPLE PREPARATION and ANNEALING

The thin film structures were prepared by vacuum deposition of the required elements on Si<> substrate, followed by furnace annealing. The details of these procedures are described under the following headings:

Wafer Preparation

The substrates for the samples were obtained by scribing and cleaving single crystal silicon wafers into 9mm x 9mm squares (10mm x 10mm for the ^{31}Si tracer experiments). Wacker silicon wafers (75mm ϕ and ca. 380μm thick) of crystal orientation <100> were used throughout this investigation. The wafers were lightly boron doped (p-type silicon) of resistivity > 1 Ω-cm.

After cleaving the samples were labelled for identification then cleaned and degreased by ultrasonic washing in methanol, acetone, trichloroethylene, acetone, and again methanol. The methanol was then removed by rinsing in deionised water (resistivity better than 10 MΩ-cm) and the samples etched for 5 min. in 20% hydrofluoric acid (HF) to remove the native oxide layer. Following established techniques the samples were then oxidized for 5 min. in RCA

solution (H_2O_2:NH_4OH:H_2O :: 1:1:5) and re-etched in 6% HF. The RCA etch was omitted in samples where the substrate was not intended to participate in the reaction. At this stage the samples were clean enough to be lifted dry out of the final solution. After careful inspection they were mounted on the aluminium sample holders for immediate loading into the evaporating chamber.

Vacuum Evaporation

To achieve the high vacuum desired for evaporation a number of different pumps were used. For the roughing stage a rotary pump reduced the pressure to about 10^{-1} torr. A liquid nitrogen (LN_2) trap prevented backstreaming of oil from the pump. A pair of LN_2 cooled molecular absorption pumps then reduced the pressure to approximately 10^{-4} torr, at which point the ion pumps could be used. The ion pumps subsequently reduced the pressure to better than 10^{-6} torr. Immediately prior to evaporation a LN_2 filled cryopanel further improved the vacuum to about 10^{-7} torr. During evaporation a Ti sublimation pump was activated to maintain good vacuum (10^{-6}-10^{-7} torr). Pressures were measured with a thermocouple gauge down to 10^{-2} torr, and a Penning gauge at lower pressures.

Evaporation was accomplished by electron beam heating of the metal or silicon chips, located in a water cooled copper hearth. The system had three such hearths, each of which

could be moved into position without breaking vacuum, to allow choice of evaporated material.

Furnace Annealing

Samples were vacuum annealed in a Lindberg quartz tube furnace with a digital temperature controller. A turbo-molecular pump assisted by a LN_2 cryopanel kept the pressure below 10^{-6} torr during annealing. Temperatures and times were dictated by experimental requirements, but were generally in the range 250 to 750 °C and 5 to 80 min. The system contained a carousel accommodating eight quartz boats which could be sequentially loaded into the furnace without breaking vacuum. Each boat could hold up to 5 samples.

2.2 RUTHERFORD BACKSCATTERING SPECTROSCOPY

Rutherford backscattering spectroscopy (RBS) is a well established tool for the analysis of thin film structures and was the major analytical method used in this investigation. A brief review of the concepts involved is given below. A more comprehensive treatment is given in ref. 59.

When a low energy particle beam is directed onto a target, the particles are elastically scattered, recoiling with energies given by, $\acute{E} = kE_0$, where E_0 and $\acute{E}$ are the energies before and after scattering, and k, the kinematic factor, is given by

$$k = \left((1-\mu^2 \sin^2\theta)^{1/2} + \mu\cos\theta \right)^2/(1+\mu) \qquad (2.1)$$

where θ is the scattering angle (in the laboratory frame of reference), and μ is the mass ratio, $M_{projectile}/M_{target}$. Thus for a given scattering geometry and projectile, k depends only on the target mass, so that the energy kE_0 uniquely identifies the sample atoms.

In Fig. 2.1 a particle beam of energy E_0 is shown directed onto a thin sample at an angle ϕ to the normal. Particles of energy kE_0 scattered from the surface are detected at an angle β to the normal (scattering angle, $\theta = 180° - (\beta+\phi)$). The number of particles scattered is relatively small so the beam continues, essentially unattenuated, into the sample. Scattering occurs at all levels within the sample, with particles scattered from the rear of the sample being detected with energy E_1. The particles lose energy due to interaction with the sample electrons as they traverse the sample, both on the inward and outward paths, so that E_1 is necessarily less than kE_0. The energy difference, $\Delta E = kE_0 - E_1$, is a measure of the thickness of the sample.

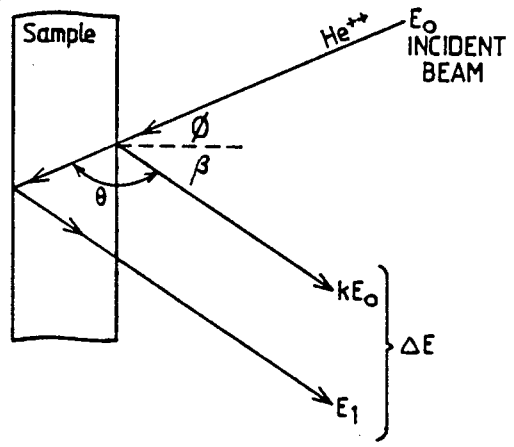

Figure 2.1 RBS schematic showing angles and energies referred to in the text.

To obtain quantitative results it is necessary to know the specific energy loss dE/dx of the particle beam in the sample; dE/dx depends on the particle identity and energy, and on the composition and density of the sample. As theoretical methods to determine dE/dx have not been successful the values at different energies have been measured experimentally and are available as tabulated data, in the form of stopping cross sections, ϵ, where

$$\epsilon \equiv (1/N)(dE/dx)$$

and N is the atomic density. For this investigation, data due to Ziegler[60] were used. To facilitate computation, Ziegler fitted a function of the form

$$1/\epsilon = 1/\epsilon_{LOW} + 1/\epsilon_{HIGH}$$

to the data, where

$$\epsilon_{LOW} = A_1 E^{A2} \quad \text{and} \quad \epsilon_{HIGH} = (A_3/E)\ln(1+A_4/E+A_5E).$$

Having a function dE/dx(E) (= Nϵ), allows the thickness of a layer to be determined by

$$x = \int dx/dE\ dE = \int (1/(dE/dx))\ dE \qquad (2.2)$$

However use of this equation to determine x is complicated by the fact that in general the energy E immediately prior to scattering is not known, and also because the function 1/(dE/dx) cannot be integrated analytically. Various approximate methods have hence been developed to find x.

If dE/dx is approximated as constant over each of the inward and outward paths then

$$x/\cos\phi = (1/(dE/dx)_{|E=EIN})(E_0-E)$$

and

$$x/\cos\beta = (1/(dE/dx)_{|E=EOUT})(kE-E_1)$$

where angles and energies are as given in Fig. 2.1. Eliminating the unknown, E, from these equations gives

$$x = \Delta E/[S] \qquad (2.3)$$

where [S] is the energy loss factor:

$$[S] = (k/\cos\phi)(1/(dE/dx)_{|E=EIN}) + (1/\cos\beta)(1/(dE/dx)_{|E=EOUT}).$$

In the "surface energy approximation", E_{IN} is taken as E_0 and E_{OUT} as kE_0, which approximations are only suitable for very thin layers.

In the "mean energy approximation" the values:

$$E_{IN} = \tfrac{1}{2}(E+E_0) \quad \text{and} \quad E_{OUT} = \tfrac{1}{2}(kE+E_1)$$

are assumed. E here is still unknown, but can be estimated by various means.

For the purpose of this investigation a computer program was developed which eliminated errors due to computation altogether. The value of E was first estimated from the surface and mean energy approximations, then the function 1/(dE/dx) was integrated numerically between E_0 and E, and between kE and E_1 to obtain two values for x. E was then suitably adjusted and the process repeated successively until the two values of x were the same. Although this sounds lengthy, the algorithm converged very rapidly so that the computer produced the required result almost immediately.

RBS works equally effectively for multi-elemental layers or multi-layered samples. For samples with multiple layers the detected particles from the lower layers have lower energies due to loss in the overlying layers. Adjusting for this is simple once the thickness of the upper layer(s) is determined as above.

Layers composed of more than one element are treated according to Bragg's rule, which effectively states that each atomic species acts independently on the particle beam, so that stopping cross sections (ϵ) are additive; viz. for compound M_xSi_y:

$$\epsilon^{MxSiy} = x\epsilon^{M} + y\epsilon^{Si}$$

and

$$(dE/dx)^{MxSiy} = N^{MxSiy}\,\epsilon^{MxSiy},$$

where N^{MxSiy} is the volume density of the molecular units M_xSi_y, in the compound.

In the practical application of RBS the detected particles are scaled according to energy and stored in a multi-channel analyzer, to give a spectrum of yield (number of counts) against channel number (energy). The relative yield depends on the concentration of the target atoms and on the cross section σ, for elastic scattering for the particular projectile/target combination. For scattering angles close to 180°

$$\sigma \propto Z^2_{\text{projectile}} \cdot Z^2_{\text{target}} \cdot E^{-2}$$

Thus the relative concentrations of the constituent elements

of a layer can be directly determined from the heights of the RBS spectrum. e.g. for Ni_2Si

$(Z_{Ni}/Z_{Si})^2 = (28/14)^2 = 4$ and [Ni] : [Si] = 2:1

so that the nickel signal is expected to be 8 times that of the silicon. Similarly for NiSi and $NiSi_2$ ratios of 4:1 and 2:1 are expected respectively.

To illustrate these concepts Fig 2.2 shows a simulated 2 MeV α-particle spectrum for 2000 Å NiSi on a silicon substrate, with $\theta = 165°$ and sample angle $\phi = 10°$. The signals from the different elements are identified and the energies and yields discussed above indicated. The thickness of the layer may be determined from either ΔE_{Ni} or ΔE_{Si}.

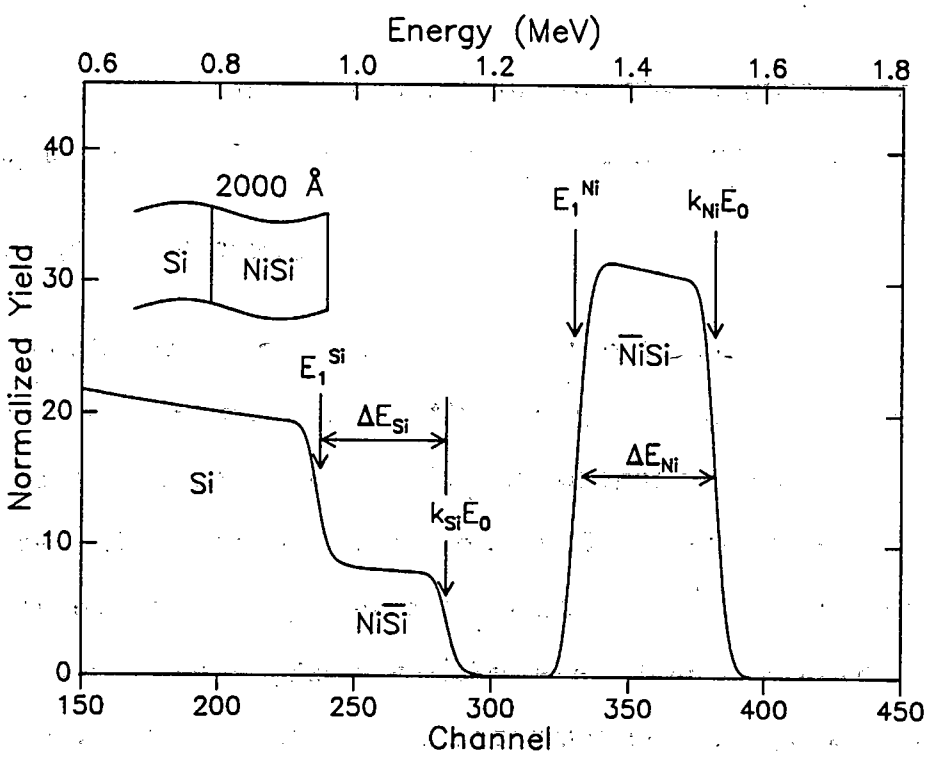

Figure 2.2 Simulated 2 Mev α-particle RBS spectrum of Si/2000 Å NiSi/, showing energies referred to in the text.

this procedure is clarified by the following more specific discussions.

Activation and Acquisition of the ^{31}Si

The radioactive silicon was produced by overnight irradiation of ultra-pure (99,999%) silicon at the reactor facility of the Atomic Energy Board at Pelindaba. A thermal neutron flux of the order of $2,5.10^{13}$ neutrons cm^{-2} s^{-1} was maintained, producing ^{31}Si by the nuclear reaction $^{30}Si(n,\gamma)^{31}Si$. The high purity of the silicon ensured the absence of significant quantities of spurious active isotopes.

^{30}Si has a natural abundance of only 3,1% and since the neutron capture cross section is low (0,1 b), only a minute fraction of the silicon became activated. Typically about 200 mci of activity was produced in 5 g of silicon on each occasion.

The activated silicon was removed from the reactor early in the morning and flown immediately to Cape Town, being received in the laboratory at Faure at about 2 p.m. on the same afternoon. The pump down process to achieve good vacuum in the evaporating chamber is time consuming, but it was generally possible to begin evaporating procedures at about 10 p.m. that night.

Decay of ^{31}Si

^{31}Si decays with a half-life of 2,62 hours by the emission of β^- particles (E_{max} = 1,48 Mev) for 99,93% of its disintegrations, to produce the stable isotope, ^{31}P. Since the absolute quantity of ^{31}Si was extremely small it is unlikely that the presence of the daughter product ^{31}P had any influence on the reaction.

The short half-life of ^{31}Si is highly advantageous as radiation hazards accompanying its use are short lived. It also however required the completion of the experiments while useful activity remained; i.e. within about 24 hours of removal from the reactor. It was usually possible to analyze three sets (of 10 each) of samples in the period from midnight to mid-morning, at which time the activity was too low to be of further use.

Activity Counting

The activity was measured using a Geiger-Müller arrangement with a pulse shaper and scaler. Counting period was 5 min., giving counts of the order of 3000 (ca. 2% statistics) for a virgin sample. The background count (ca. 180 c.p.m.) was subtracted and each count extrapolated back to a common time datum using the decay law, $N_0 = N.\exp(\lambda t)$. The decay of the ^{31}Si activity was monitored by periodic counting of a reference sample. By comparing counts before and after sputtering, the percentage activity remaining after removal of silicide was obtained.

R.F. Sputtering

Microsectioning of samples was achieved by ion beam sputtering with Ar^+ plasma. The Ar^+ plasma was produced by R.F. ionization of spectroscopically pure Ar, at 12,33 MHz, using 100 - 150 W of power. The Ar was introduced into the sputtering chamber via a needle valve to a pressure of about 6.10^{-3} torr (base vacuum ca. 10^{-6} torr). The samples were glued to the water cooled cathode using Ag paste for good thermal and electrical contact. Using this arrangement sputter rates of the order of 100 - 150 Å/min were obtained.

Since the samples were backscattered and activity counted both before and after sputtering, the percentage activity remaining after removal of a known thickness of silicide was determinate. By sputtering each sample for a different time the integral of the activity profile , for a given sample structure and heat treatment, could be constructed.

Evaluation of Si^* Thickness

To properly interpret the results of these experiments it is crucial to determine the thickness of the layer of Si^* deposited. The expected concentration profile for a particular diffusion mechanism can only be calculated if this is known. RBS is effectively insensitive to Si and Si^* differences, and better accuracy was desired than provided by the evaporation crystal monitor. The following procedure was consequently developed:

Approximately 1500 Å of Si^* was evaporated onto a 4 x 4 cm square of light Al foil. The thickness of Si^* on the foil was determined both by RBS, and by precision weighing (to 0,02 mg precision) on a Mettler analytic balance, before and after deposition. The two methods generally gave results within 5% agreement. The foil was then cut into 16 squares, each approximately $1cm^2$, a few of which were weighed and activity counted. The activity count was normalized to $1cm^2$ according to the mass of each foil square, and an average normalized count obtained.

Each sample was weighed and counted before sputtering, allowing a similar area normalized average count to be calculated for each set of samples. The Si^* thickness on each set of samples was deduced from the known thickness on the foil by comparing average normalized activity counts.

2.4 INERT MARKER TECHNIQUES

In the inert marker experiments the marker, which consisted of a very thin (5 - 10 Å) metal layer, was evaporated onto the sample in the appropriate position. The depth of the marker within the structure was subsequently determined by computer analysis of the RBS spectrum, both before and after annealing.

In deciding upon a marker to use the points mentioned in section 1.10, concluding that the experiments did not warrant excessive effort, were taken into account.

Consequently such techniques as ion beam implantation, or island structure type markers, were rejected, and a simple uniform layer of metal decided upon. Molybdenum and tantalum were chosen as the metals for the following reasons:-

(i) They both form silicides, but only at temperatures above that required for the nickel silicides being studied (650 °C for $TaSi_2$ and 525 °C for $MoSi_2$)[9] so that they could reasonably be considered *inert* markers.

(ii) Their solubility in silicon is not excessive so that they would not suffer significant diffusion into the structure.

(iii) They both have relatively high atomic mass, making their position, in very thin layers, readily identifiable by RBS techniques.

(iv) Neither Mo nor Ta had previously been used as markers in the analysis of nickel silicide formation

(v) They were both available in the laboratory for immediate use.

Tungston was also considered as a possibility, but was finally rejected in favour of the others as its extremely high melting point makes it difficult to deposit by evaporation techniques.

The techniques, simple though they were, proved adequate and good results were obtained, as evidenced in the following chapters.

CHAPTER 3

DIFFUSION DURING Ni_2Si FORMATION

3.1 INTRODUCTION

Diffusion during the growth of Ni_2Si was investigated experimentally using both ^{31}Si tracer and inert marker techniques. The ideas behind these experiments have been discussed already in some detail in Sections 1.8 and 1.7 respectively, and the experimental methodology was reviewed in chapter 2. For convenience the basic concepts are reiterated briefly below. After presentation of the experimental results the implications thereof are considered in the discussion of results.

3.2 EXPERIMENTAL

^{31}Si Tracer experiments

Following the procedures outlined in chapter 2, samples with the structure Si<100>/Si(a)/Si^*/Ni (where Si^* indicates the radioactive Si) were prepared, and annealed to form Ni_2Si and Ni_2Si^*. After annealing the integral of the activity profile was determined by sputter microsectioning and activity counting. The thickness of the Si^* layer was estimated by activity comparison with a layer of measured thickness on aluminium foil.

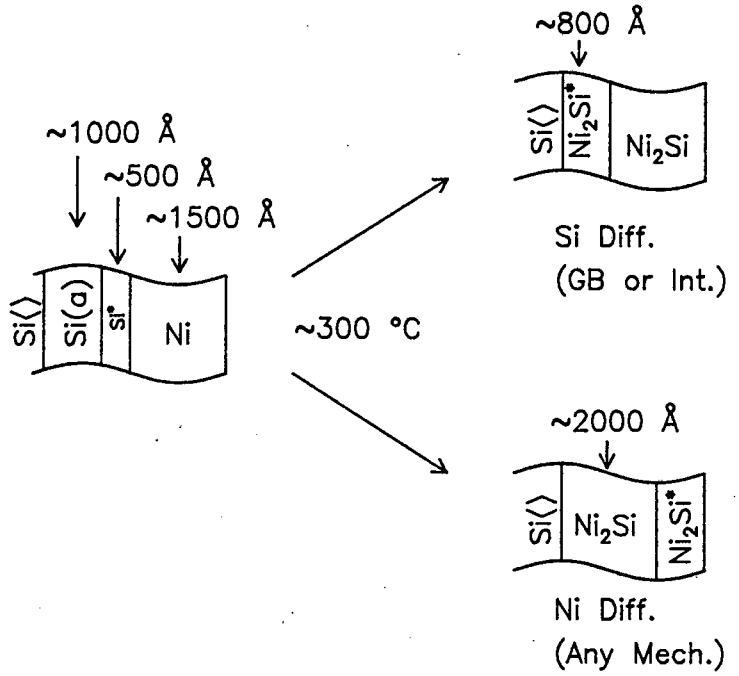

Figure 3.1 Basic Ni_2Si Si^* tracer experiment. The final position of the Si^* layer is determined by the diffusing species and mechanism. Approximate experimental parameters are enumerated. Exact values are given in Table 3.1.

Fig 3.1 illustrates how the diffusion mechanism and diffusing species may be inferred from the final position of the Ni_2Si^* layer. For silicon GB or interstitial diffusion the Ni_2Si^* layer lies beneath the Ni_2Si layer, whereas for nickel diffusion (any mechanism) it moves to the surface.

The Ni_2Si ^{31}Si tracer experiment was performed a number of times; the results of two of these (Exp. 3.1 & 3.2) are presented here. The numerical values of some relevant experimental parameters are included in Fig 3.1, and are listed more comprehensively in Table 3.1.

Table 3.1 Ni_2Si ^{31}Si Tracer Experimental Parameters. Thickness values are given in Å.

Parameter		Exp. 3.1	Exp 3.2
Si^* on Al foil	: (Nom.)	1600	1650
	: (RBS)	1450±90	1360±90
	: (Mass)	1522±30	1410±30
	: (Mean)	1500±30	1400±30
Si^* on samples	: (Nom.)	400	550
	: (Calc.)	405±10	520±16
Ni_2Si^*	: (Calc.)	680±20	870±30
Total mean Ni_2Si	: (RBS)	2125±55	3000±15
Annealing	: Temp. (°C)	300	310
	: Time (Min.)	30	30
Sputter Rate (Å/Min.)		152±25	145±12

Inert Marker Experiments

Two marker experiments, Exp. 3.3 and 3.4, were performed on Ni_2Si growth, using tantalum and molybdenum as markers respectively. The markers were vacuum deposited as a thin continuous layer 5-10 Å thick beneath the nickel. To be consistent with the ^{31}Si tracer experiment amorphous silicon was provided below the marker for reaction with the nickel. The resultant structures (Si<>/Si(a)/M/Ni) were annealed for 30 min. at temperatures between 300 and 330 °C, to produce partial or complete Ni_2Si growth. Marker position before and after annealing was determined by RBS.

Fig 3.2 shows the sample structure before annealing, and after complete Ni_2Si formation. For silicon diffusion the marker is always expected to be below any Ni_2Si formed (and

any remaining Ni), whereas for nickel diffusion the marker remains above the Ni_2Si but below any remaining nickel.

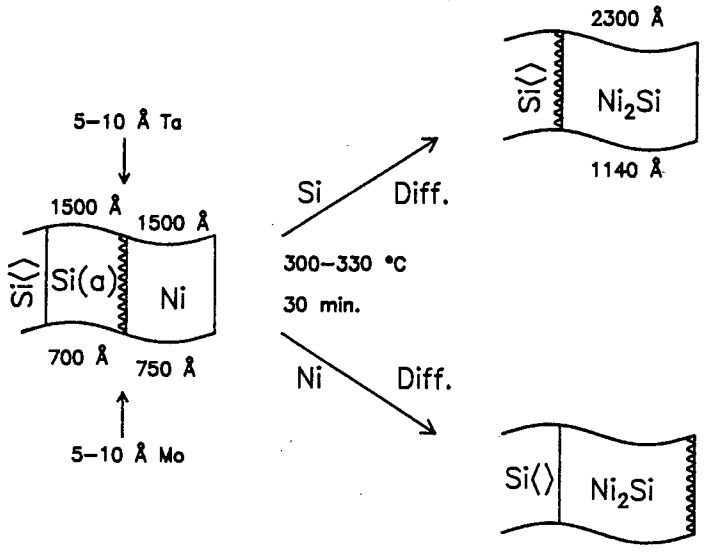

Figure 3.2 Ni_2Si inert marker experimental concept. The final position of the marker depends on the diffusing species. Layer thicknesses (Ta Exp. above, Mo below), and annealing parameters used in the experiments are given.

3.3 RESULTS

^{31}Si Tracer Experiments

Fig 3.3 shows typical RBS spectra (from Exp. 3.1) of the Ni_2Si after 0-5 min. of sputtering. The sputtering process can be seen to have effectively removed Ni_2Si from the samples without significantly affecting the remaining silicide.

The sputter rate curves for the two experiments are shown in Fig. 3.4. Sputter rate was approximately 150 Å/min., although considerable scatter of the points about the mean

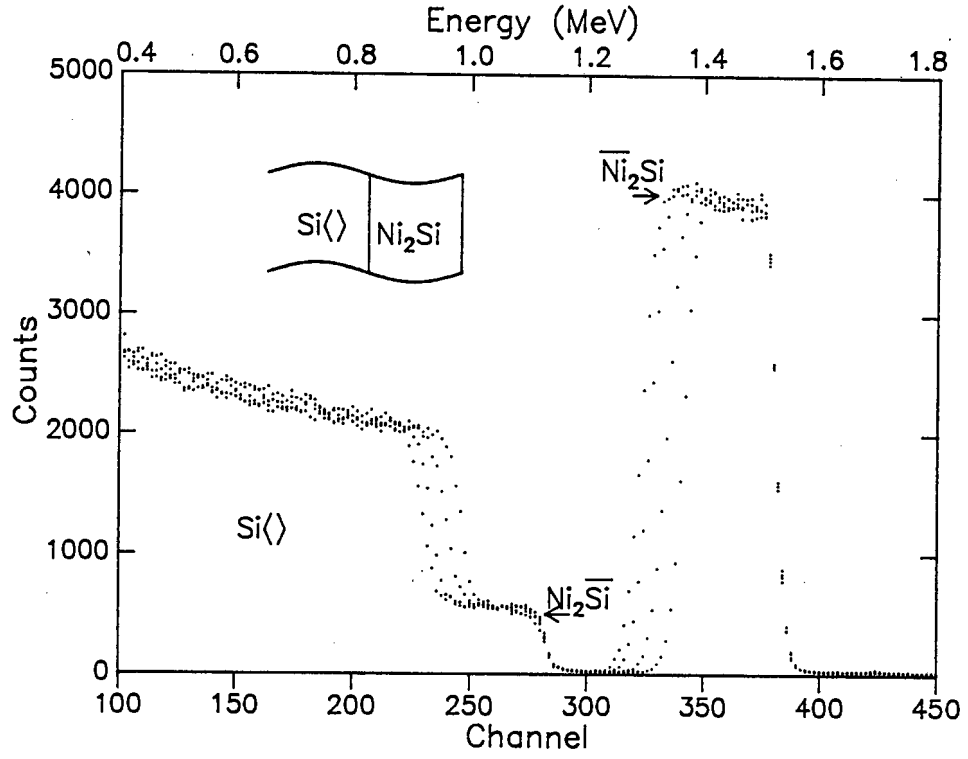

Figure 3.3 2 Mev α-particle RBS spectra of Exp 3.1 samples after sputtering for 0-5 min. Thinning of the Ni_2Si layer by the sputtering process is evident.

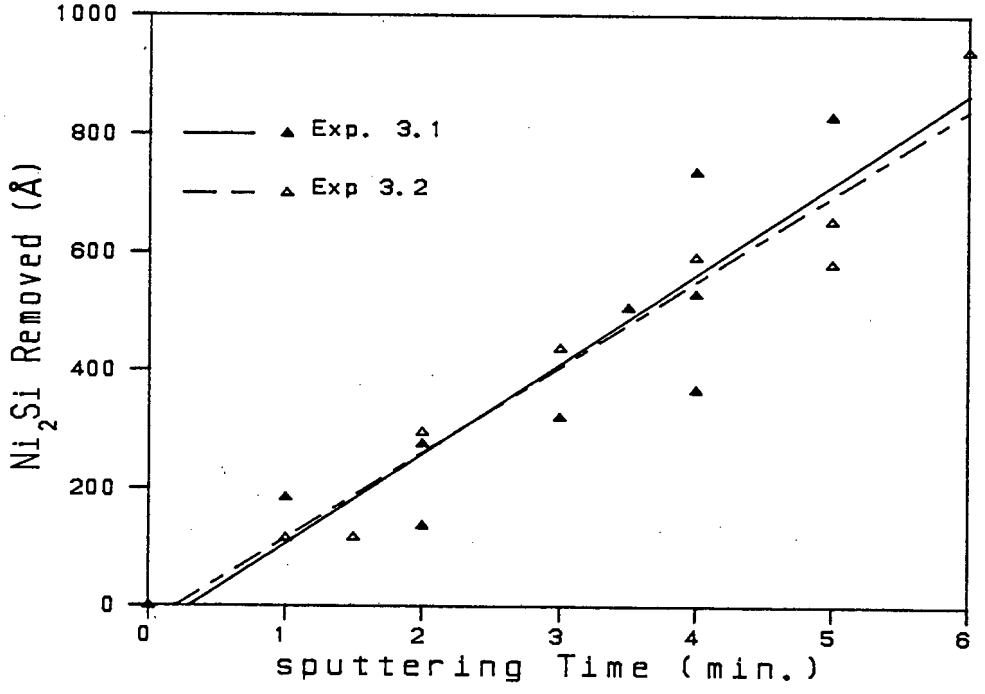

Figure 3.4 Sputter curves for Exp's 3.1 and 3.2. The data for Exp. 3.2 shows less scatter as all the samples were backscattered both before and after sputtering.

line is evident; this is attributed, at least partially, to the considerable uncertainty in the determination of the thickness of silicide removed. It is evident that Exp. 3.2 showed less scatter (and hence less uncertainty in sputter rate) than Exp. 3.1, an expected result due to the somewhat improved techniques used for the latter experiment. In Exp 3.1 the initial Ni_2Si thickness was assumed to be that of an unsputtered reference sample, introducing an estimated ±2% (of the *total* initial silicide thickness) additional error (i.e. ~ ±50 Å). In Exp. 3.2 each sample was backscattered before and after sputtering, eliminating this source of error.

The final results ot the experiments are shown in Fig. 3.5 (a) (Exp 3.1), and (b) (Exp. 3.2). These plots of residual activity vs Ni_2Si removed represent the integral of the activity profiles, and are expected to be linear for an Ni_2Si^* layer of uniform activity. Also shown in each figure are the expected results for silicon (GB or interstitial) diffusion and for nickel diffusion. For silicon diffusion by GB or interstitial mechanisms the Ni_2Si^* layer is expected to be below the Ni_2Si layer so the residual activity should remain at 100% as the upper surface layers are removed. For nickel diffusion (by any mechanism) the Ni_2Si^* layer is expected to be on the surface, and the residual activity is thus expected to decrease linearly as Ni_2Si^* is removed. Two lines are drawn on each plot showing the expected result

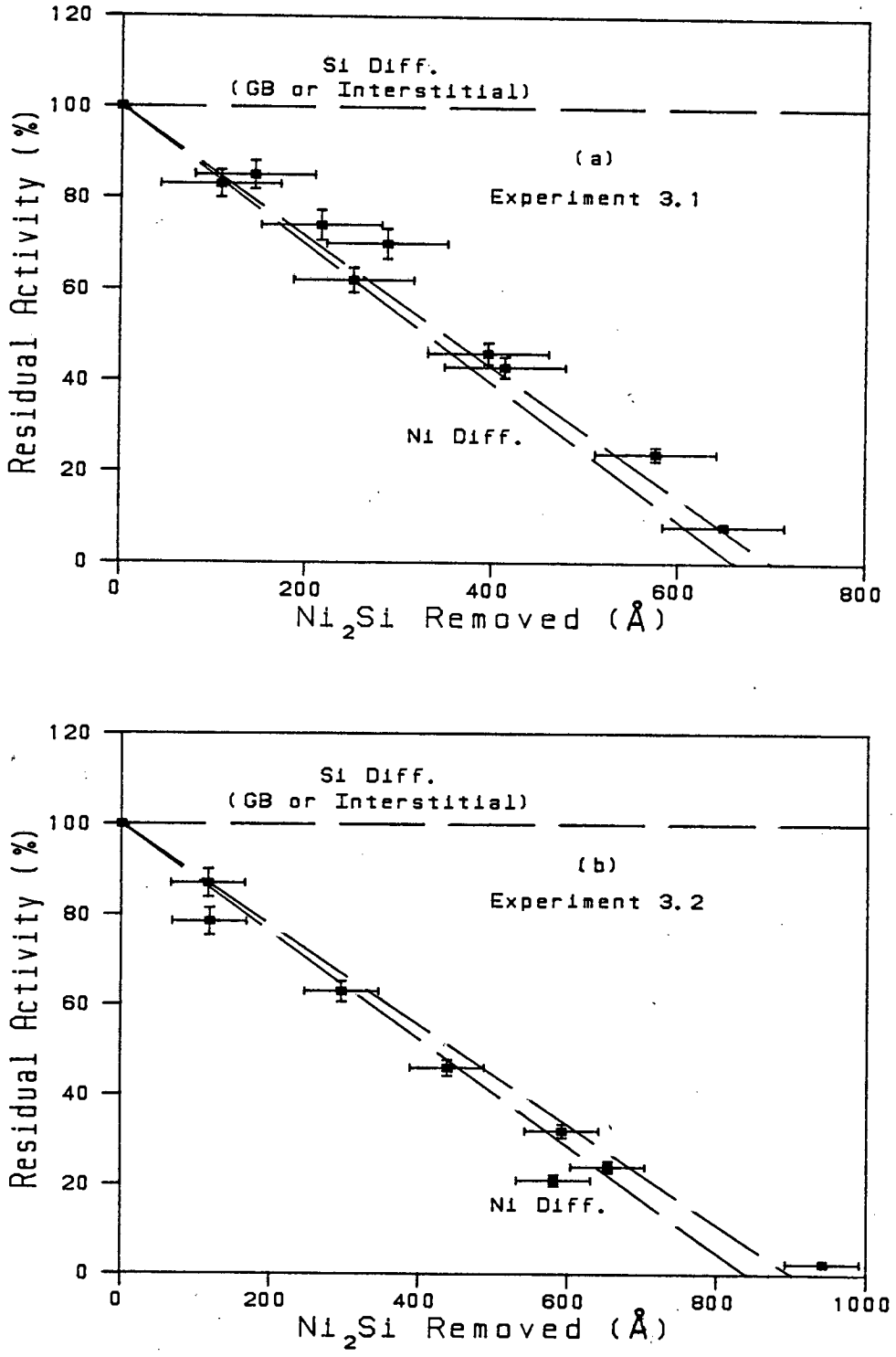

Figure 3.5 Measured activity profile integrals for Ni_2Si growth. The dashed lines show the expected result for Si or Ni diffusion. The pair of lines drawn for nickel diffusion is indicative of the uncertainty in the estimated Ni_2Si^* layer thickness.

following nickel diffusion, with the channel so formed representing the estimated uncertainty in the calculated thickness of the Ni_2Si^* layer (resulting from the uncertainty in the estimated Si^* thickness, cf. Table 3.1).

The experimental points plotted include error bars as uncertainty estimates. The vertical error bars are derived from the statistical uncertainty in activity counting and are, perhaps contrary to expectation, smaller where the percentage residual activity is least, and lower counts are obtained. The vertical fractional uncertainty in each point is however still greatest at the lower activity points, even though the size of the error bars tends to obscure this. The horizontal error bars represent the uncertainty in the estimation of the thickness of Ni_2Si removed. This was estimated at ±1 channel (i.e. 4 keV ~ 35 Å) of the RBS spectra for both before and after sputtering. The error bars in Fig. 3.5 (b) are somewhat smaller due to the improvement in experiment technique described above. Slightly less scatter in the points is evident.

The experimental points in both Fig. 3.5 (a) and (b) are seen to fall, within experimental error, along the expected line for nickel diffusion. In Fig. 3.6 the results of the two experiments have been normalized and plotted together. In this figure the mean expected line for nickel diffusion (dashed line, slope = -0,115 %/Å), and a linear regression on the experimental points (solid line, slope = -0,111 %/Å),

have also been plotted. The results conclusively show that nickel diffusion occurred during Ni_2Si growth.

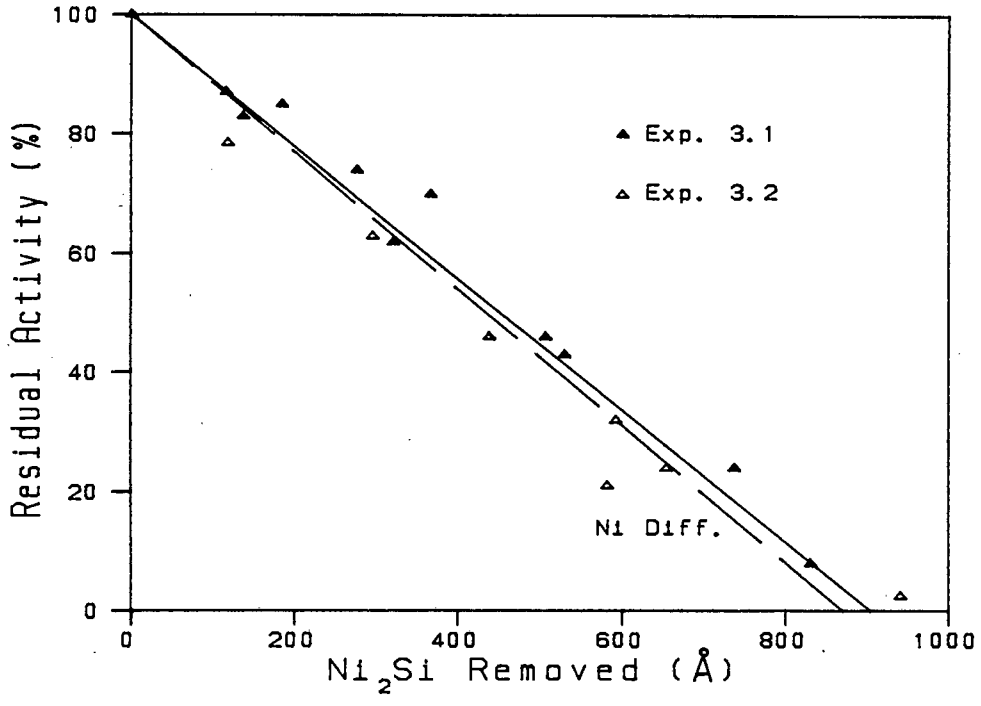

Figure 3.6 Overall Ni_2Si ^{31}Si tracer results. The results of Exp 3.1 have been normalised to fit those of Exp 3.2. The dashed line shows the calculated mean expected result for nickel diffusion; the solid line is a linear regression on all the experimental points.

Inert Marker Experiments

(i) Tantalum Marker

Figure 3.7 shows RBS spectra of virgin and partly grown Ni_2Si samples. The growth of Ni_2Si is evident, as is the shift of the marker towards the surface. The Ta surface position is also marked. The marker movement towards the surface is consistent with nickel diffusion.

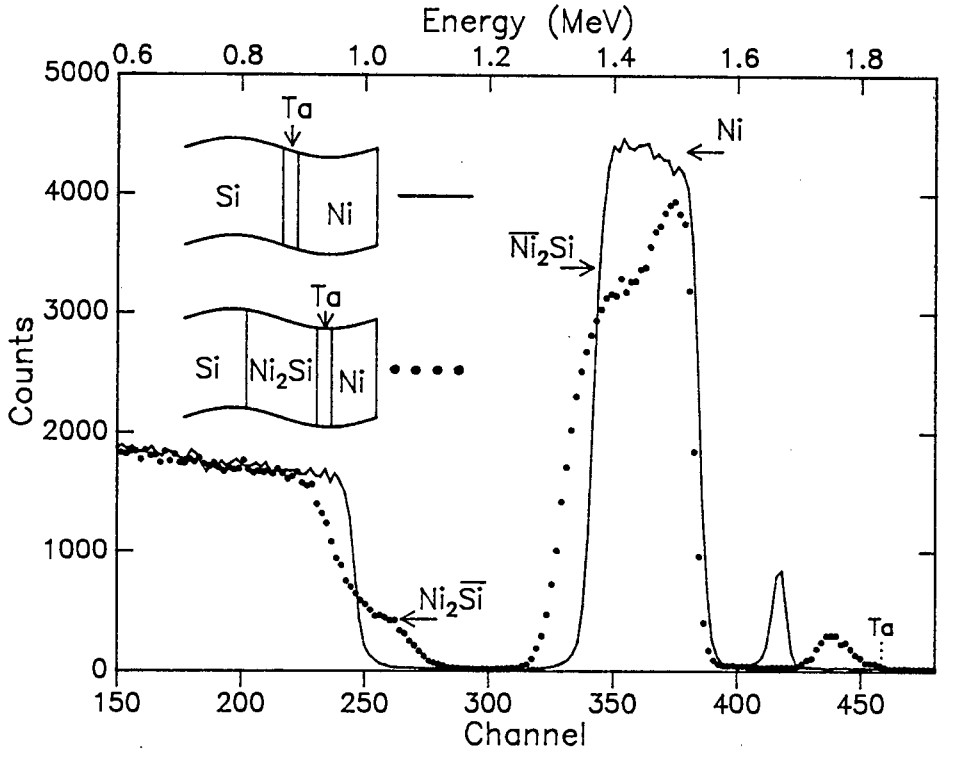

Figure 3.7 2 MeV α-particle RBS spectra of Ta marker samples, before Ni_2Si growth and after partial Ni_2Si formation. The movement of the marker toward the surface, consistent with nickel diffusion, is clear.

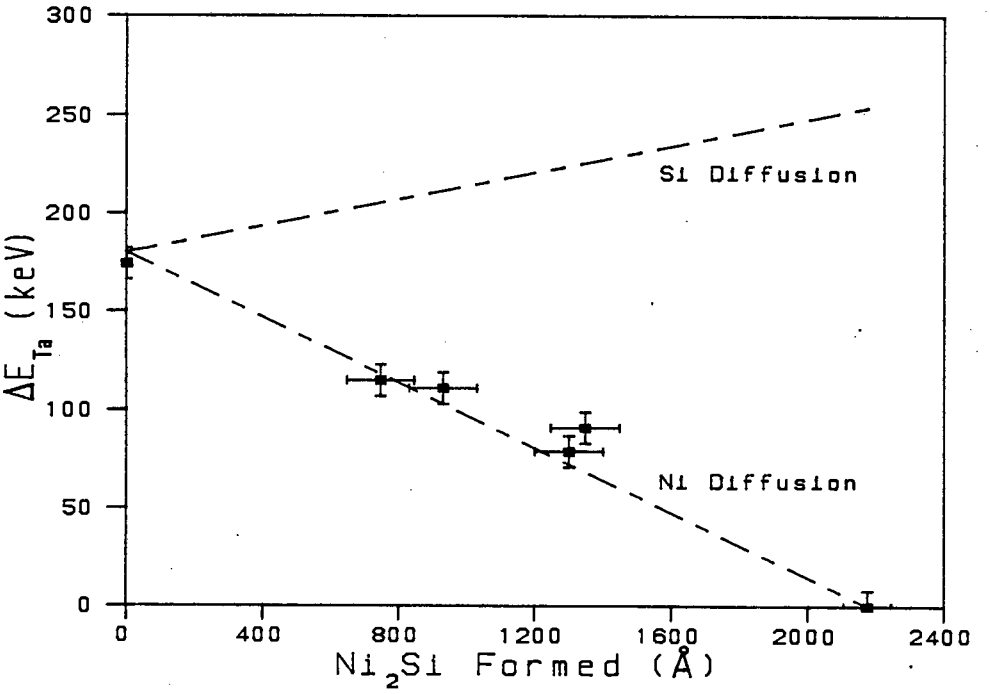

Figure 3.8 Ta marker Ni_2Si results. ΔE_{Ta}, the energy shift of the Ta marker from its surface energy, is plotted against Ni_2Si formed. Marker movement closely follows that expected for nickel diffusion.

The final result for the experiment is shown in Fig. 3.8. Here ΔE_{Ta}, the energy shift of the marker from its surface position, is plotted against growth of Ni_2Si. Also shown are lines representing the expected marker movement for nickel diffusion and for silicon diffusion. The vertical error bars represent the uncertainty in the estimation of marker RBS energy (taken as ±2 channels ~ ±8 keV). The horizontal error bars were determined from the estimated uncertainty in the amount of Ni_2Si grown. This was fairly large (±3 channels ~ ±100 Å) for the partly grown Ni_2Si samples due to the difficulty of estimating actual Ni_2Si thickness from spectra of samples where unreacted nickel still remained (e.g. see Fig. 3.7). In all samples where complete growth occurred the marker was found at the surface.

Marker movement shown in Fig. 3.8 is seen to closely follow the expected line for nickel diffusion. The results are consistent with nickel being the diffusing species during Ni_2Si growth.

(ii) Molybdenum Marker

Mo has a lower atomic mass (96) than Ta (181) and consequently a lower RBS surface energy (1697 vs 1833 kev for 2 Mev RBS). It was thus necessary to perform the Mo marker experiment with much thinner nickel and Ni_2Si layers (750 Å Ni and 1140 Å Ni_2Si) to prevent obscuring of the marker RBS signal by the Ni signal. The thickness

measurement of partly formed Ni_2Si layers is impractical with such thin layers, so it was not possible to produce results in the form of Fig. 3.8 for the Mo experiment. The results are best inferred directly from the RBS spectra.

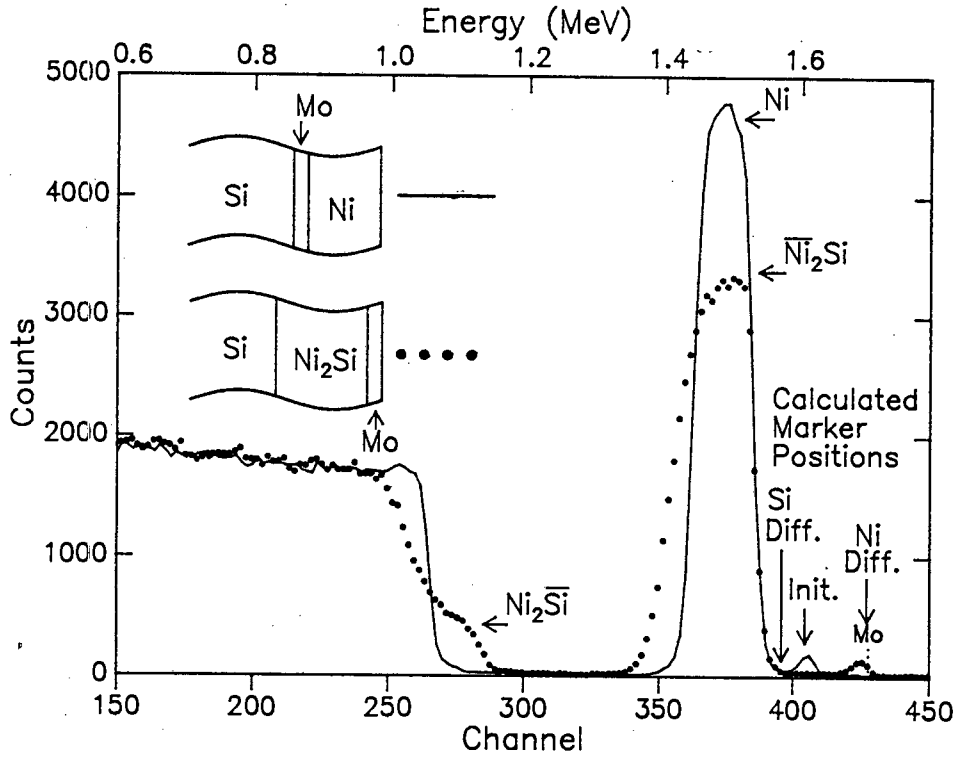

Figure 3.9 Mo marker Ni_2Si results. 2 MeV α-particle RBS spectra for virgin, and completely grown Ni_2Si samples are shown. Calculated marker positions for the virgin sample (Init.) and for Ni and Si diffusion are indicated. The marker can be seen to have moved to the expected position for nickel diffusion.

Figure 3.9 shows RBS spectra for virgin, and completely formed Ni_2Si samples. Also shown in this figure are the calculated positions of the marker in the virgin structure, and in the final structure for either silicon or nickel diffusion. Marker movement is clearly consistent with nickel diffusion. The Mo marker experiment thus also indicates nickel as the diffusing species.

3.4 DISCUSSION OF RESULTS

Figures 3.5 and 3.6 represent the final results of the ^{31}Si tracer experiments on Ni_2Si growth. These plots of residual activity vs silicide removed are the integrals of the activity profiles. The results are presented in this way because this is what is actually measured by the experimental procedure. To produce the activity profiles required to correlate results with diffusing species and mechanism, according to Fig. 1.11 and 3.1, the results must be differentiated. In Fig. 3.6 a straight line has been fitted to the data, giving the profile shown in Fig. 3.10.

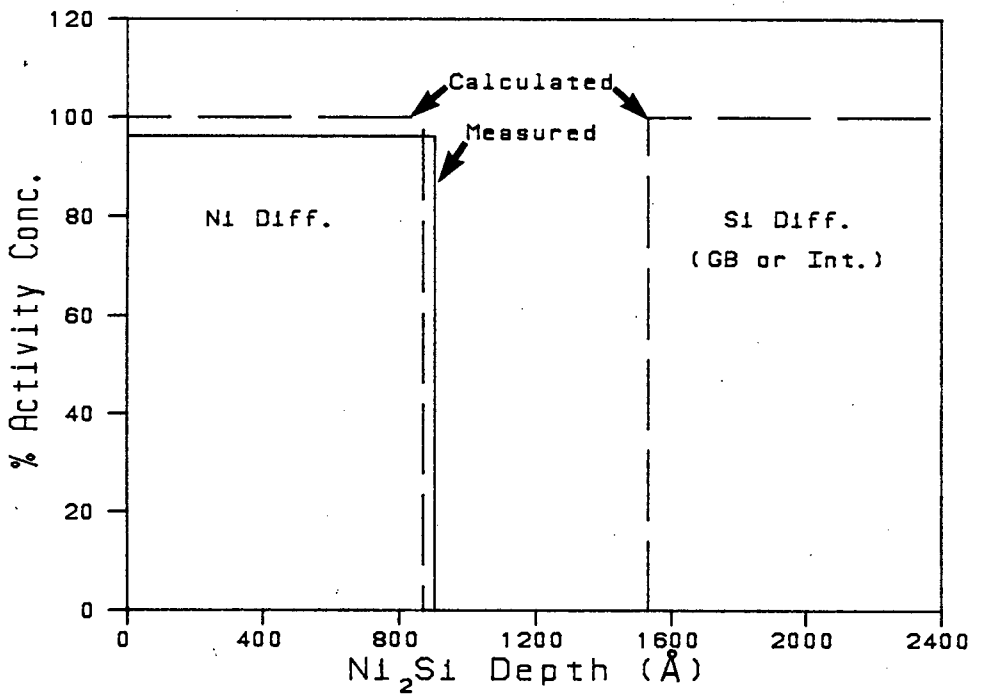

Figure 3.10 Si^* Activity profile for Ni_2Si ^{31}Si tracer experiment obtained from the assumed straight line fit to the experimental data.

Calculated profiles for nickel or silicon diffusion are also shown. The measured profile corresponds closely to that expected for nickel diffusion. The difference between the calculated and measured profiles is considered to be within experimental uncertainties and is thus not significant.

Care must be exercised in the interpretation of the results as presented in Fig. 3.10. The square profile shown is a consequence of the use of a linear fit to the data of Fig. 3.6, and is not intended to imply that the profile is exactly this shape. Although the straight line is a good fit to the data of Fig. 3.6, and its use a reasonable assumption on theoretical grounds, it is obvious from the uncertainties of the data points and their scatter about the line, that the choice of functions to fit to the data is wide open. As the differentiation process tends to magnify errors each choice of function produces a radically different activity profile (illustrated further in Section 4.4). The precise shape obtained for the activity profile is thus to a large extent an artifact of the curve fitting procedure. The important implications of Fig. 3.10 are, (i) that the *average* concentration (over a few hundred or so Å) corresponds closely to that expected for nickel diffusion, and (ii) that all the activity is within the expected thickness of Ni_2Si following nickel diffusion. The experiments have thus clearly and convincingly established nickel as the diffusing species in these reactions.

The results of the previous experiment of this type performed by Pretorius et al[50] were reproduced in Fig. 1.13, and discussed in section 1.9. The results showed an activity level of approximately 60% in the Ni_2Si^* layer, a result which was apparently inconsistent with later work on NiSi (Ref. 31) (Section 1.9). The current results *are* consistent with previous NiSi results; the Si^* activity remains at 100% throughout the Ni_2Si^* layer and shows little spreading. One of the primary objectives of this work, which was to investigate this problem, has thus been successfully accomplished.

The results obtained here are also consistent with the only other tracer study performed on Ni_2Si, that due to Baglin et al[55], in which ^{56}Ni was used as the active isotope. In their experiment Ni_2Si was formed by annealing Si<100>/Ni^*/Ni structures at 350 °C. The resultant Ni^*_2Si profiles were somewhat diffuse, but essentially in the correct position for nickel diffusion. It was concluded that Ni_2Si growth occurs by nickel vacancy and GB diffusion, in roughly similar proportions. In a Si^* experiment any type of nickel diffusion should give the profile shown in Fig. 3.10, so this is clearly in agreement with the present results.

The inert marker experiments used an ultra-thin but continuous layer of Mo or Ta as the marker. While the marker was found to move in the correct direction it must be noted that the only absolute conclusion which can be inferred is

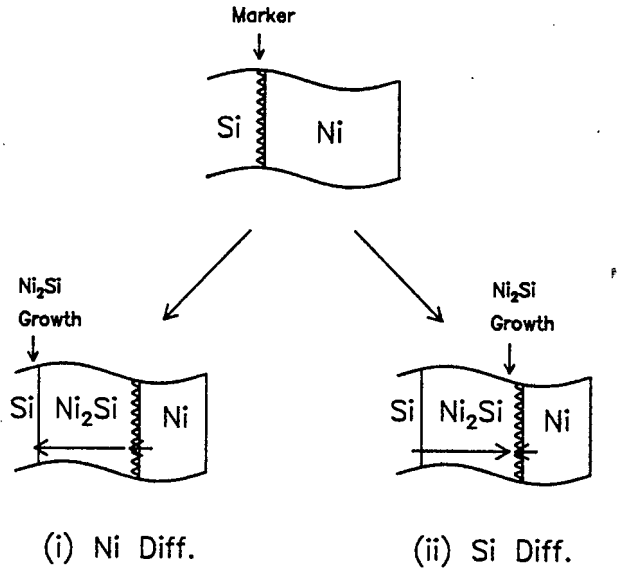

Figure 3.11 Marker movement towards the surface proves conclusively only that Ni diffused through the marker. In (i) silicide growth occurs by Ni diffusion and in (ii) by Si diffusion. Both show identical marker movement.

that the nickel diffused through the *marker* (or vica versa). The extension of the argument to conclude that nickel diffused through the partly formed Ni_2Si is an assumption, albeit a reasonable one. This point is illustrated in Fig. 3.11. In (i) silicide growth occurs by nickel diffusion, while in (ii) silicon diffusion occurs. In both cases nickel diffuses through the marker giving identical marker movements. Some improvement to the experiment could have been affected by burying the marker partly in the Ni_2Si layer, but the growth could still have been severely influenced by the diffusion properties of nickel and silicon in the marker. It is observed however, from the spreading of the marker RBS signal (Fig. 3.7 and 3.9), that the marker layer was considerably more diffuse after silicide growth; this is considered to be an indication that the marker layer was broken up during silicide growth. Subsequent diffusion

could then occur between marker grains, and growth would be less influenced by the diffusion properties of Ni and Si in the marker. Growth of silicide by Si diffusion as shown in Fig. 3.11 (ii) is then less likely to have occurred, and the assumption that the observed marker movement indicates that growth occurred by Ni diffusion (Fig. 3.11 (i)) is reasonable. The inert marker experiments have thus confirmed nickel as the diffusing species (Fig. 3.8 and 3.9).

Marker experiments have previously been performed on Ni_2Si using Ag[38], W[39], and Xe[34-37]. In all of these experiments nickel has been found to be the sole diffusing species. Xe marker experiments are performed by ion implantation of Xe atoms within the structure, and the question of nickel or silicon solubility within the marker does not arise. Diffusion in Ni_2Si growth has thus been very extensively investigated with inert marker techniques, and this present work, using previously unused markers of Ta and Mo layers, is in agreement with the exclusive result that nickel is the diffusing species.

In conclusion it may be stated that ^{31}Si tracer and Ta and Mo inert marker experiments performed have shown that Ni_2Si forms with nickel as the diffusing species. The experiments could not determine the mechanism of diffusion. The current results are consistent with previous Si* work on second phase NiSi growth, and also with other published inert marker investigations of Ni_2Si growth.

CHAPTER 4

DIFFUSION DURING NiSi FORMATION

4.1 INTRODUCTION

Diffusion during NiSi growth from $NiSi_2$ and silicon was investigated using ^{31}Si tracer and inert marker techniques. The concepts of these experiments and their application to second phase growth were discussed in section 1.8 and 1.7, and the experimental details were given in chapter 2. The format of this chapter parallels that of chapter 3, beginning with a brief account of the experimental details and concepts, followed by the presentation, and finally the discussion, of results.

4.2 EXPERIMENTAL

^{31}Si Tracer Experiment

The second phase ^{31}Si tracer experiments began the same as that for first phase, with the preparation and annealing of Si<>/Si(a)/Si^*/Ni structures. The annealing temperature was higher (400 °C) so that NiSi grew after formation of Ni_2Si. R.F sputter microsectioning was used to profile the final activity. The original thickness of the Si^* layer was determined as before, by comparison of sample activities with that of a measured thickness of Si^* on aluminium foil.

For second phase evaluation it is required that a layer of uniform concentration of Ni_2Si^* first be produced on the surface of the sample. In chapter 3 it was shown that this occurs naturally as a result of nickel diffusion during Ni_2Si growth. The Si^* concentration in this layer may be calculated from the estimated initial Si^* thickness, allowing the expected activity profile after NiSi growth to be determined.

Figure 4.1 illustrates how the mechanism and species during second phase growth is inferred from the final $NiSi^*$ profile. In this case it is the concentration of the Si^* in the $NiSi^*$ layer that is affected by the mechanism and species during diffusion.

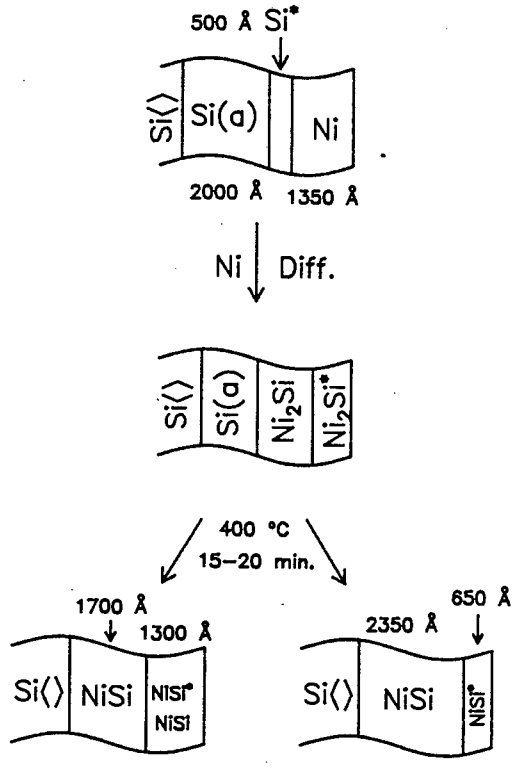

Figure 4.1 NiSi ^{31}Si Tracer experiment. The concentration of the Si^* in the surface layer of $NiSi^*$ is determined by the diffusion mechanism and species. Layer thicknesses and annealing parameters are included.

Table 4.1. NiSi ^{31}Si Tracer Experimental Parameters. Thickness values are given in Å.

Parameter		Exp. 4.1	Exp 4.2
Si^* on Al foil	: (Nom.)	1650	
	: (RBS)	1360±90	
	: (Mass)	1410±30	
	: (Mean)	1400±30	
Si^* on samples	: (Nom.)	500	500
	: (Calc.)	564±20	505±20
Ni_2Si^*	: (Calc.)	942±33	844±33
$NiSi^*$ Si Diff.	: (Calc.)	1370±50	1225±50
$NiSi^*$ Ni Diff.	: (Calc.)	685±25	613±25
Total mean NiSi	: (RBS)	2997±13	2986±23
Annealing	: Temp. (°C)	400	400
	: Time (Min.)	20	15
Sputter Rate (Å/Min.)		103±9	114±7

Two experiments on NiSi growth are presented, experiments 4.1 and 4.2. Both of these followed on from experiment 3.2, so that experimental data concerning the Si^* on the aluminium foil is identical. This data is reproduced here for convenience, together with other relevant data for experiments 4.1 and 4.2, in Table 4.1.

Inert Marker Experiments

Ta and Mo marker experiments (Exp. 4.3 and 4.4), analogous to experiments 3.3 and 3.4 on first phase growth, were also performed on NiSi growth. The markers were deposited as continuous ultra-thin (5-10 Å) layers. The virgin structures in this case included a layer of Si(a) above the marker to allow Ni_2Si growth prior to NiSi growth. The samples were

annealed at 400 °C for times between 5 and 40 min. to produce partial or complete NiSi growth. The marker position before and after growth was determined by RBS.

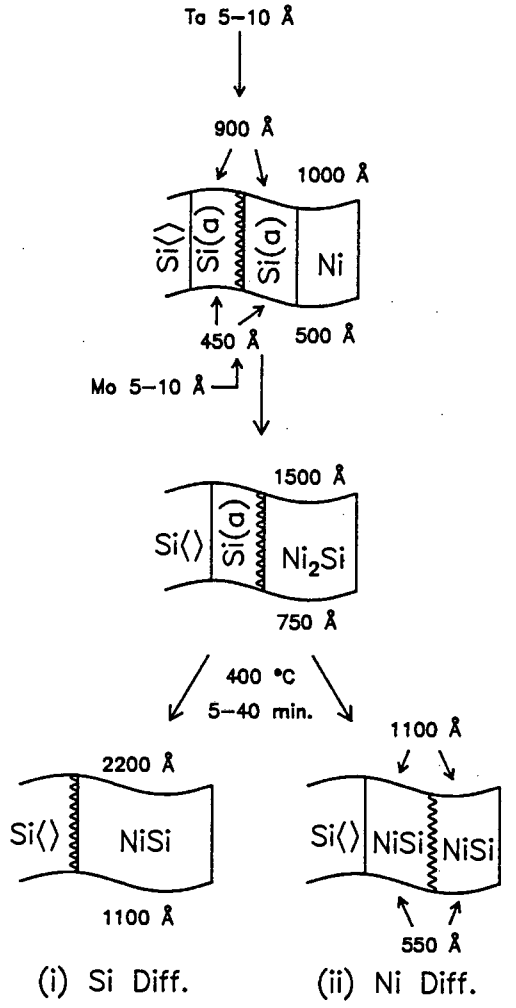

Figure 4.2 NiSi inert marker experiment. The final position of the marker depends on the diffusing species. Layer thicknesses (Ta Exp. above, Mo below), and annealing parameters are specified.

Figure 4.2 shows the sample structure before and after annealing, and the expected marker movement for each diffusing species. For second phase nickel diffusion the marker is located in the middle of the NiSi, whereas for silicon diffusion it is below the entire NiSi layer.

4.3 EXPERIMENTAL RESULTS

^{31}Si Tracer Experiments

Figure 4.3 shows typical RBS spectra (from Exp. 4.1) of the NiSi layer before sputtering, and after sputtering for 4-8 minutes. The sloping back edges of the spectra indicate poor Si/NiSi interfaces, but may also have been caused by some laterally non-uniform third phase growth (with excess Si(a)). This was not expected to affect the results as the NiSi* was located near the surface. The effect of the sputtering process on the NiSi is clear, layers being removed without affecting the remaining silicide.

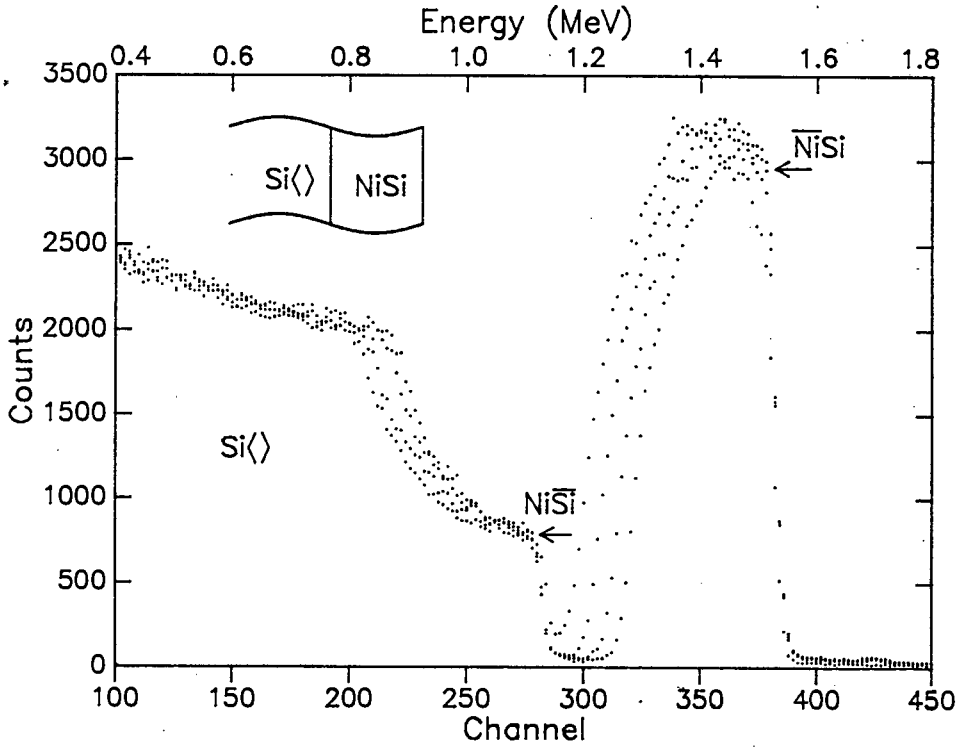

Figure 4.3 2 Mev α-particle RBS spectra of samples from experiment 4.1 after sputtering for 0-8 min. Thinning of the NiSi layer by the sputtering process is clear

The sputter rate curves for the two experiments are shown in Fig. 4.4. In both experiments 4.1 and 4.2 all samples were backscattered before and after sputtering. As discussed in the previous chapter (Section 3.3) this reduces the uncertainty in the determination of thickness of silicide removed. This improvement is reflected in Fig. 4.4 where uncertainties on the sputter rates are smaller (compare Section 3.3 Fig. 3.4 Exp. 3.1)

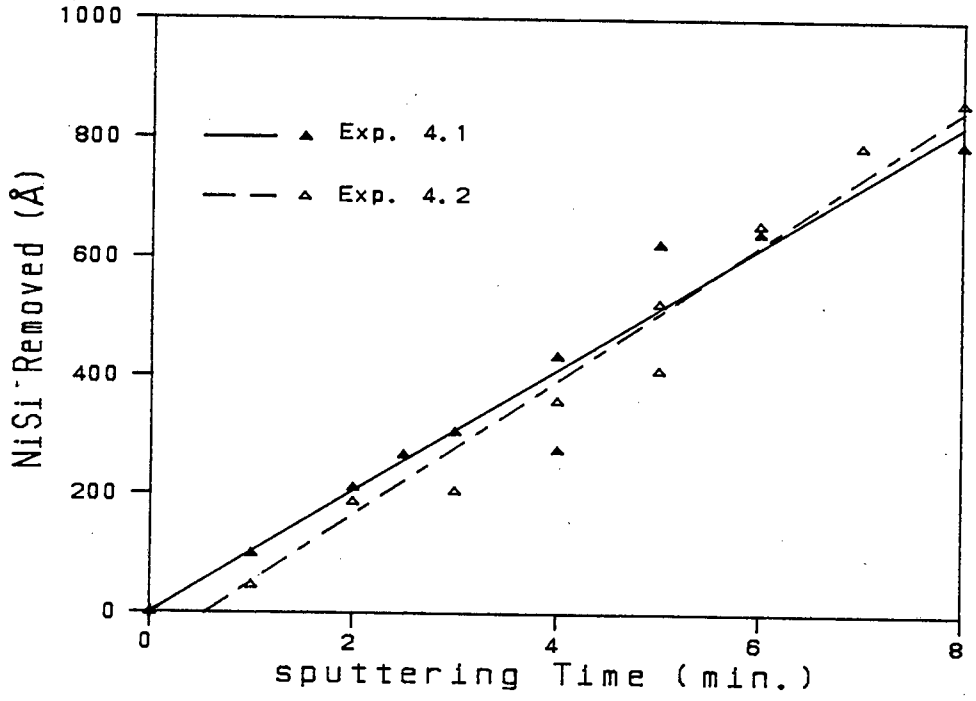

Figure 4.4 Sputter rate curves for NiSi, experiments 4.1 and 4.2

Figures 4.5 (a) and (b) represent the final results of experiments 4.1 and 4.2 respectively. These are again plots of residual activity vs silicide removed, and are expected to be linear for a layer of uniform activity. Lines reflecting the expected slope for second phase nickel or

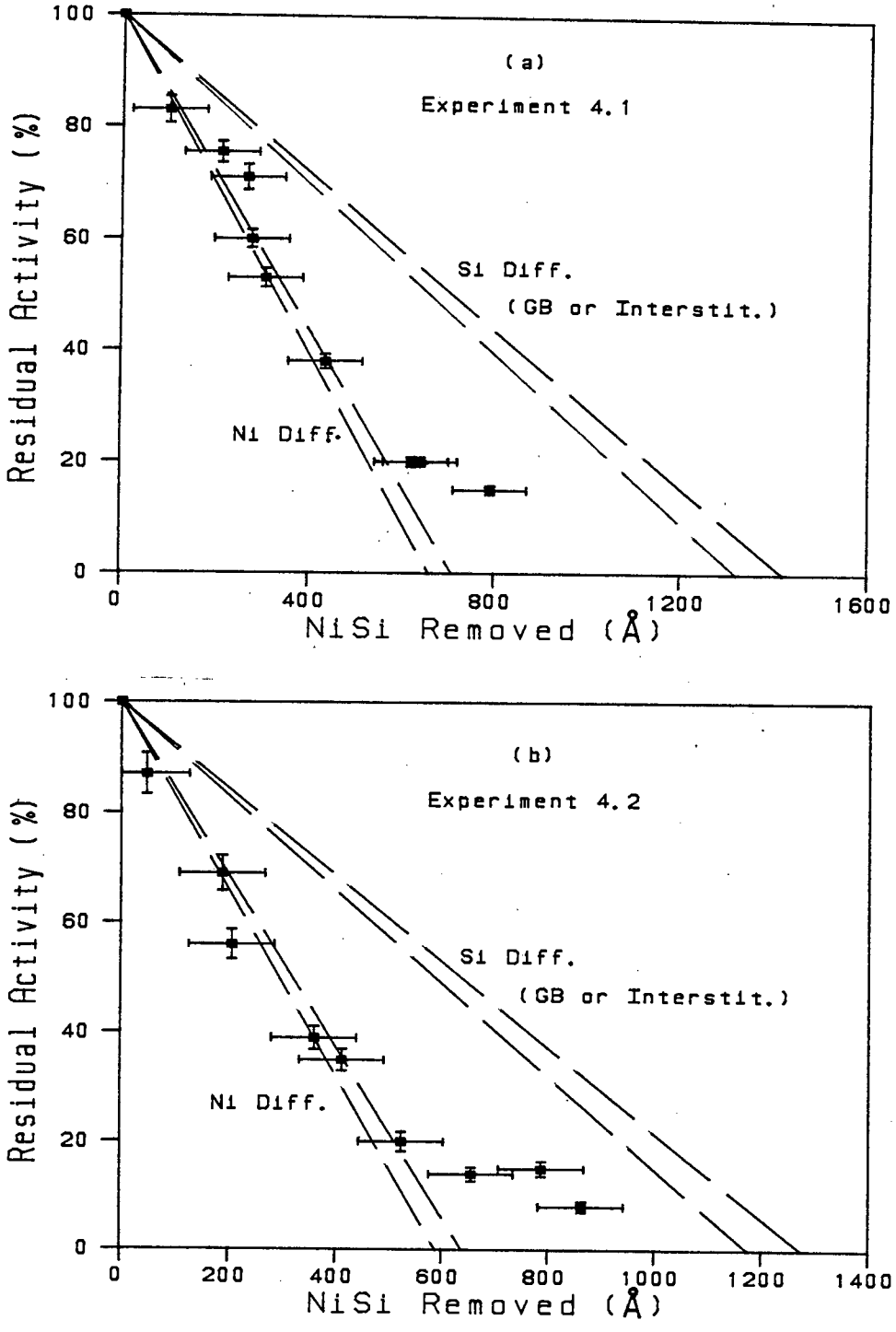

Figure 4.5 Measured activity profile integrals for NiSi growth. Expected lines for Ni and Si diffusion are shown, with each pair of lines representing the estimated uncertainty in the calculated slope.

silicon diffusion (Si vacancy excluded) are also shown, each pair representing also the estimated uncertainty in these quantities. As shown in Fig. 4.1 the $NiSi^*$ is expected to remain at the surface for both nickel and silicon diffusion, the concentration being determined by the diffusing species; this is reflected in the different slopes of the lines drawn for nickel and silicon diffusion in Fig. 4.5.

The error bars in Fig. 4.5 again represent uncertainties in measurement of activity and thickness of silicide removed. The thickness uncertainties were slightly greater in these experiments (compare Exp. 3.2 Fig. 3.5(b)) as the rounded back edge of the RBS Ni peak made energy difference evaluation difficult, and the possible onset of $NiSi_2$ growth made interpretation of the energy differences more uncertain.

It is evident in Fig. 4.5 that the measured points fall along the expected line for nickel diffusion, down to a depth of about 400 Å. In Fig. 4.6 the two experiments have been normalized and plotted together. The mean expected slope for nickel and silicon diffusion, as well as a 4th order polynomial least squares fit to the data points, are also shown. Down to about 400 Å this curve very closely follows the nickel diffusion line. The implications of fitting such a curve to the data, and the overall interpretation of the results shown in Fig. 4.6 are discussed further below.

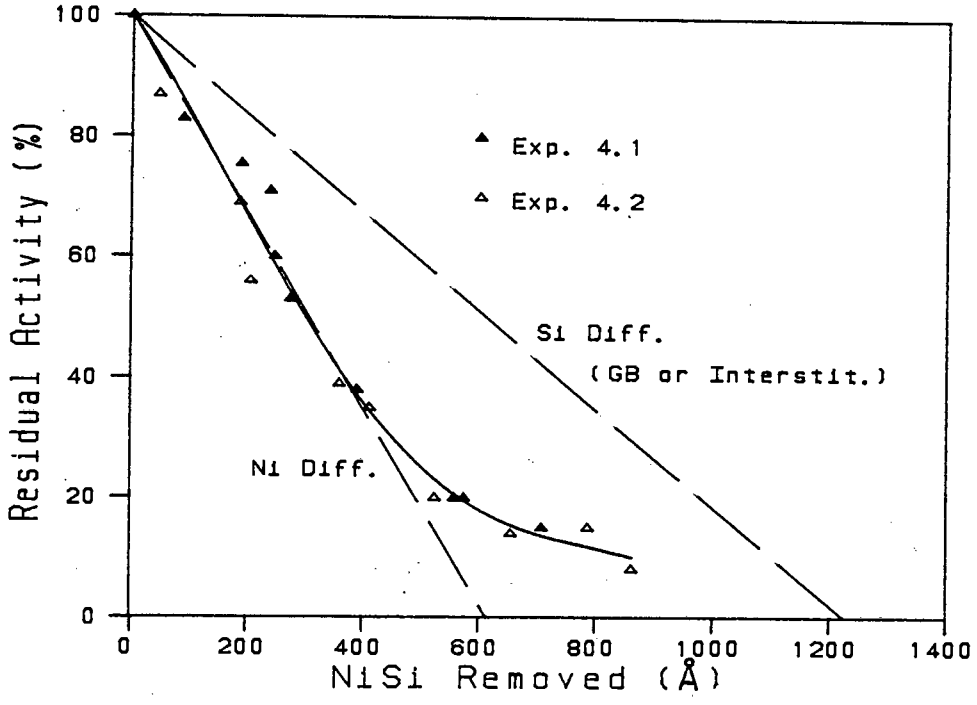

Figure 4.6 Overall NiSi ^{31}Si tracer results. The dashed lines show the mean expected results for Ni or Si diffusion. The solid line is a 4th order least squares fit to the data

Inert Marker Experiments

(i) Tantalum Marker

Figure 4.7 shows RBS Spectra for the virgin structure, and for a sample with complete NiSi growth. Movement of the marker toward the surface with growth of NiSi is clear, which result is once again consistent with nickel diffusion.

The final results of the Ta marker investigation on NiSi growth are plotted in Fig. 4.8. As for Fig. 3.8 on Ni_2Si growth, the energy shift of the marker from its surface value is plotted against thickness of NiSi formed.

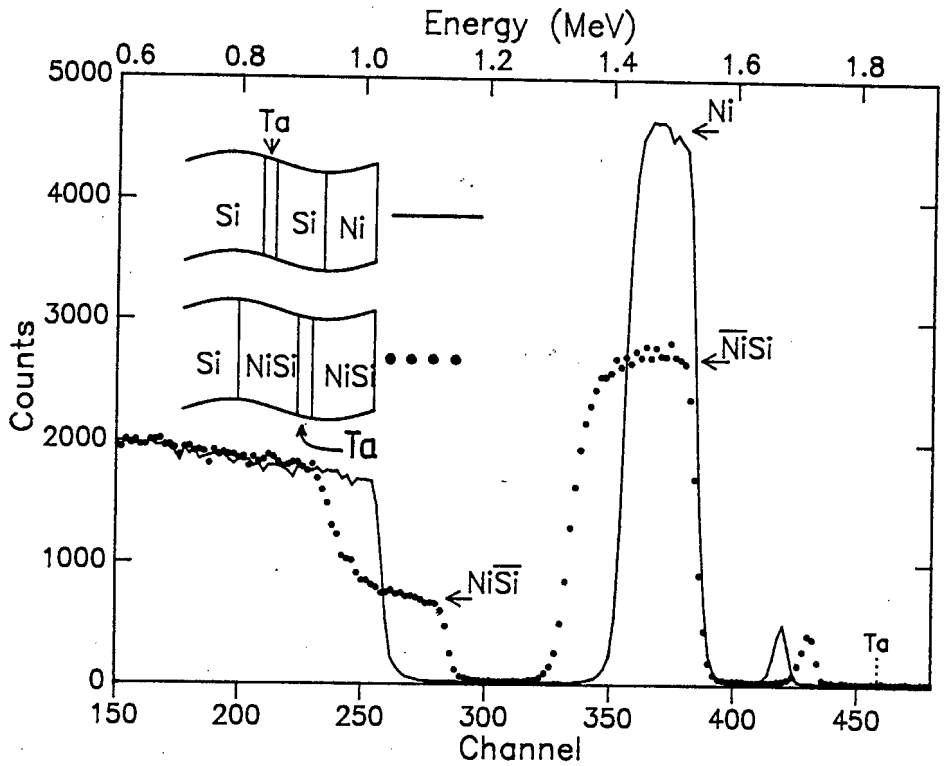

Figure 4.7 2 Mev α-particle RBS spectra of Ta marker samples, before and after annealing to form NiSi. Shift of the marker toward the surface indicates nickel diffusion.

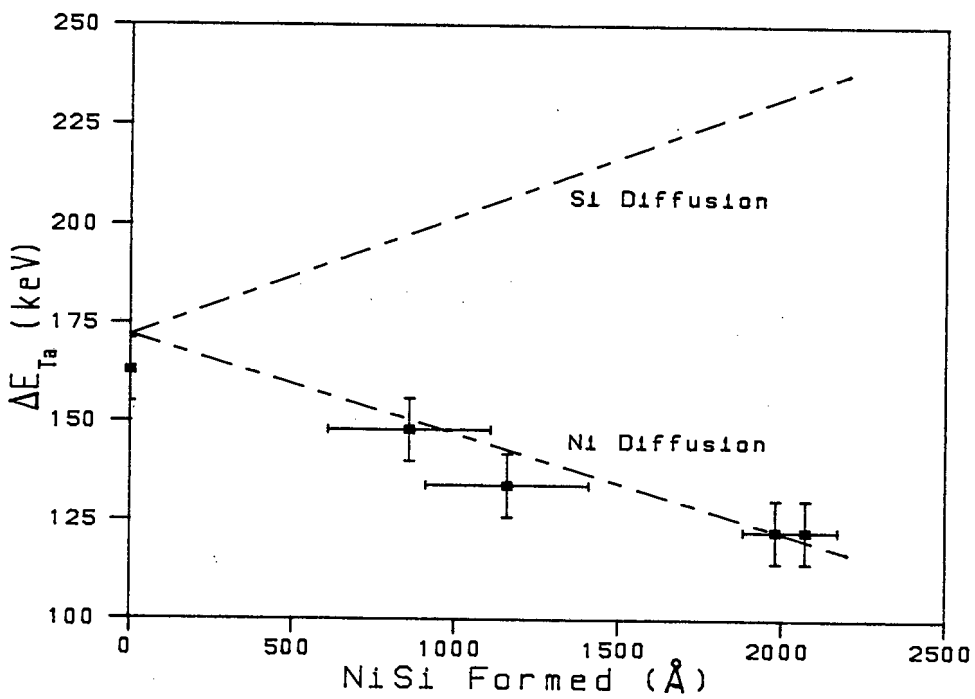

Figure 4.8 Ta marker (NiSi) results. ΔE_{Ta}, the energy shift of the marker from the surface energy, follows that expected for nickel diffusion.

Calculated lines for nickel and silicon diffusion are also shown. Vertical errors were again taken as ±8 keV. Horizontal error bars were large for the partly formed NiSi samples due to extreme difficulty in deciding the proportions of NiSi and Ni_2Si from the spectra. The actual errors were estimated by using a computer simulation program to determine the possible extremes that the RBS spectra could represent (giving ±250 Å errors). The results (Fig. 4.8) indicate nickel as the diffusing species during NiSi growth.

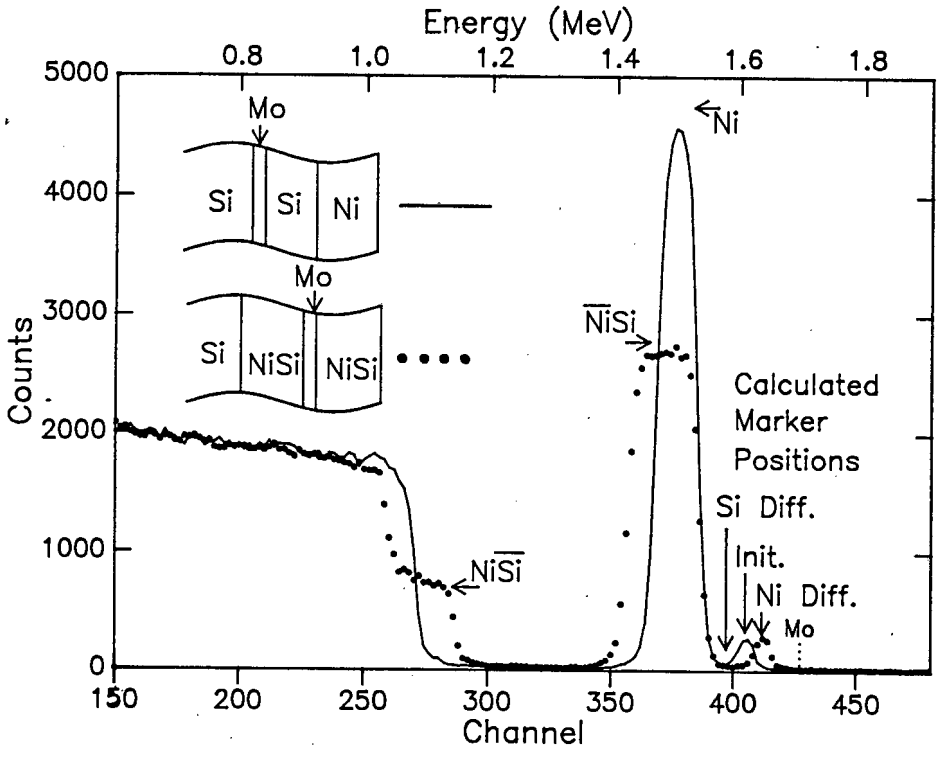

Figure 4.9 Mo marker NiSi results. 2 Mev α-particle RBS spectra for virgin and fully grown NiSi sample are shown. Calculated marker positions for virgin (Init.) and Ni or Si diffusion are indicated. Marker movement is consistent with nickel diffusion.

(ii) Molybdenum Marker

As for the Mo marker experiment on Ni_2Si (Section 3.3), the thickness of NiSi formed was necessarily too small to permit results in the form of Fig. 4.8 to be obtained. Figure 4.9 shows the RBS spectra of the samples before and after annealing. The calculated marker energies for the virgin sample (Init.), and for fully formed NiSi with nickel or silicon second phase diffusion are shown. Marker movement clearly supports nickel diffusion.

4.4 DISCUSSION OF RESULTS

The overall results of the Si^* tracer experiments are given in Fig. 4.6. This is again a plot of the concentration profile integral, so that its value at each depth is representative of the amount of activity located between the surface and that point. The mean lines for nickel or silicon (excluding vacancy) diffusion are also shown. It is apparent that the experimental data is a reasonable approximation to that expected for nickel diffusion, down to about 400 Å, subsequently deviating to higher than expected values. A curve showing a reasonable fit to the data has also been plotted. This was arbitrarily chosen as a 4th order polynomial. The differential of this function, together with those for the nickel and silicon diffusion lines, is shown in Fig. 4.10. The fitted polynomial again shows that down to a depth of about 400 Å, the activity concentration was generally consistent with that expected for nickel diffusion.

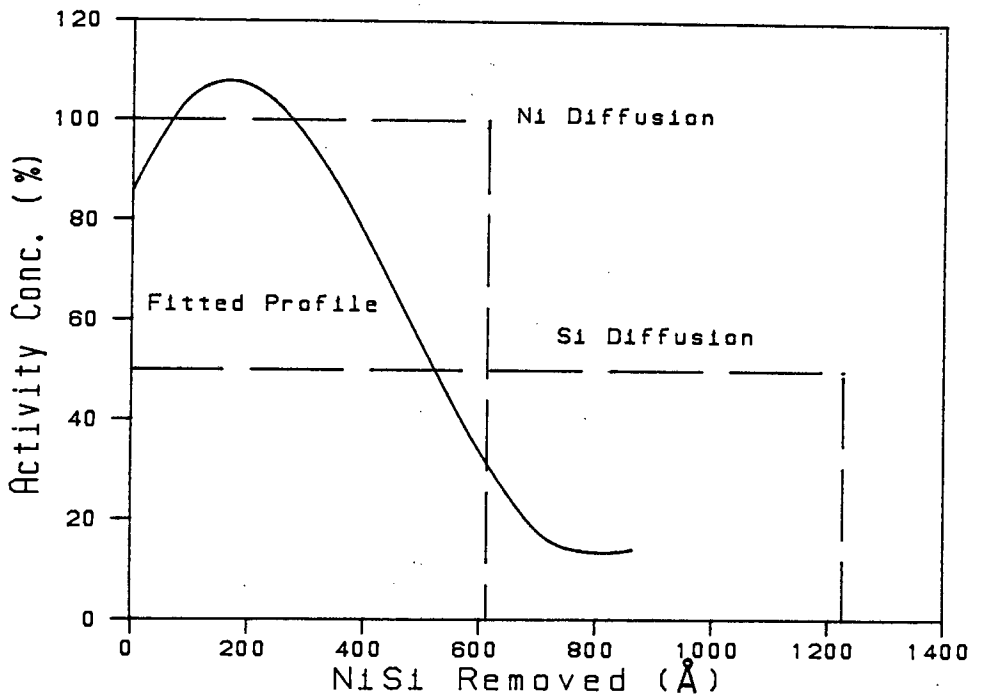

Figure 4.10 Expected activity profiles for Ni and Si diffusion (Ex. Si vacancy diff.). The fitted profile was obtained by differentiating the 4th order polynomial fitted to the experimental results of Fig. 4.6

Considering Fig. 4.10 more closely, the fitted profile is seen to have a very different shape from the ideal square profile predicted for nickel diffusion. In section 3.4 it was asserted that the precise shape of the derived concentration profile was not to be considered a firm experimental result, and this point is stressed again here. The shape of the profile in Fig. 4.10 is largely a result of the choice of a 4th order polynomial to fit the data of Fig. 4.6. Although differences between the fitted curve and the ideal nickel diffusion line (down to ca. 400 Å) in Fig. 4.6 are *barely observable*, the profiles of Fig. 4.10 are quite different. This magnification of errors resulting from the

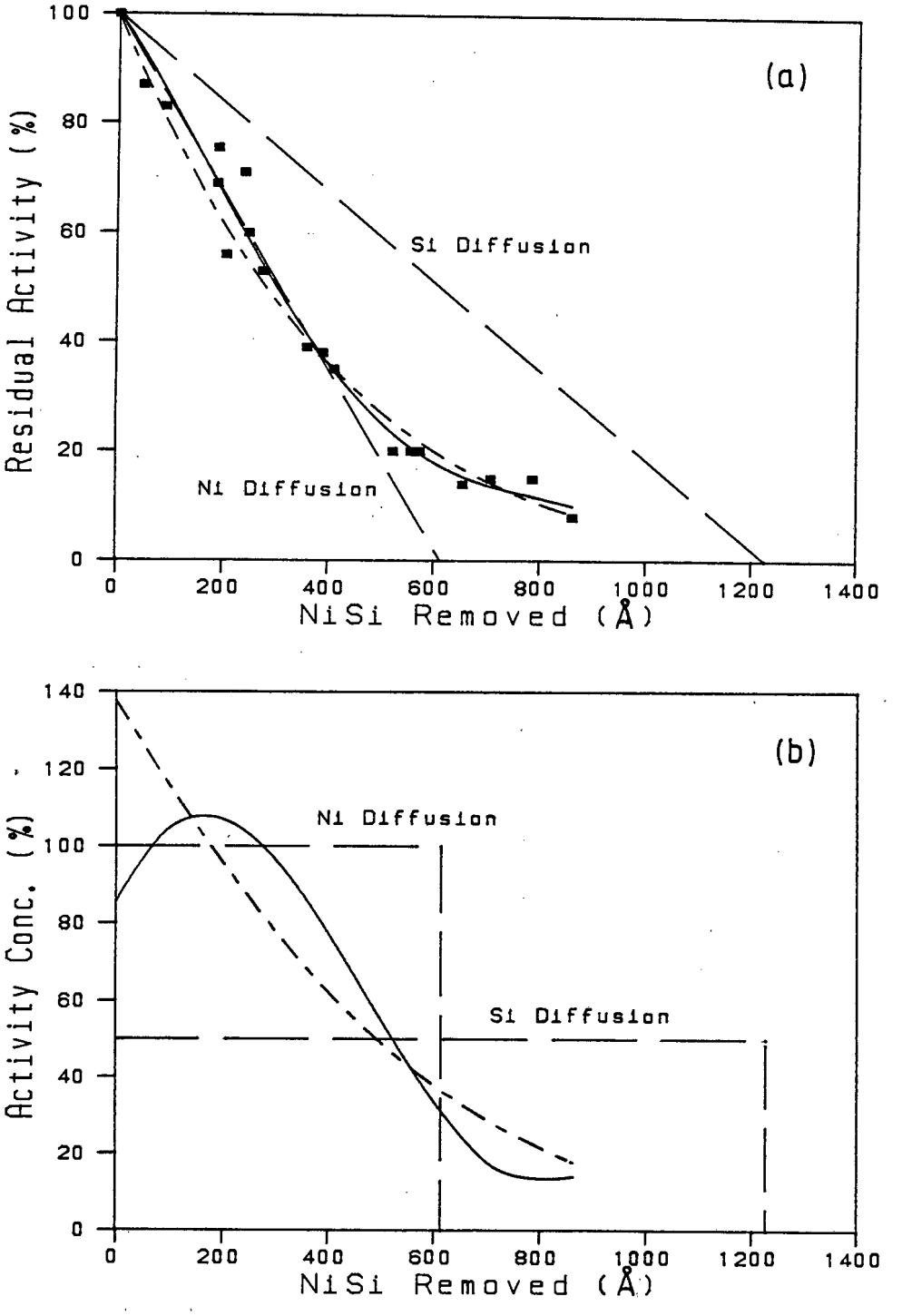

Figure 4.11 Illustration of the different profiles (b) which are obtained by differentiating different functions fitted to the data (a). In (a) the solid line is a 4th order polynomial and the dashed line is an exponential function.

differentiation process is further illustrated in Fig. 4.11. In Fig. 4.11(a) the data and 4th order polynomial fit of Fig. 4.6 have been reproduced, together with a second possible fitted curve, an exponential function (dashed line). Fig. 4.11(b) shows the vastly differently profiles obtained for these two fitted curves. Note that the exponential fit to the data is shown only to illustrate the variation in profile shape that results, and is not intended to be a reasonable alternative experimental result. (It is clear from visual inspection of Fig. 4.11(a) that the dashed curve is not as good a fit to the data as the solid curve, and the statistical parameters of the curve fitting process confirm this. Also an activity concentration of 140% as shown in Fig. 4.11(b) is quite unrealistic). It can be argued that the results (Fig. 4.6) imply an average concentration of 100% between 0 and 400 Å, and since the activity cannot exceed 100%, the profile must be flat, at 100%, down to 400 Å. It must however be remembered that the nickel diffusion line has itself an uncertainty (see Fig. 4.5), which translates to an uncertainty in the 100% position in Figures 4.10 and 4.11(b), so that profile shapes like that shown in Fig. 4.10 cannot be ruled out on these grounds. It is concluded that experimental precision is insufficient to allow the assignment of a definite shape to the concentration profile; results presented in the form of Fig. 4.10 should be taken rather as an indication of where the activity was located.

Returning to the results of Fig. 4.6 and 4.10 it is observed that down to approximately 400 Å depth the $NiSi^*$ concentration was generally consistent with that expected for nickel diffusion, but subsequently some decrease in concentration, i.e. spreading of the $NiSi^*$ occurred. This spreading is rather difficult to explain, but the following points are to be considered:

(i) If a component of silicon diffusion contributed to the silicide growth this would be expected to reduce the overall $NiSi^*$ concentration, and not just affect the region closest to the $NiSi^*$/NiSi interface. With partly silicon vacancy diffusion an overall decrease as well as spreading is to be expected. The observed spreading of the inner edge of the activity profile is thus not indicative of silicon diffusion.

(ii) A high silicon mobility would cause intermixing at the $NiSi^*$/NiSi interface, causing spreading of the profile in this region, but in this case some growth of silicide due to silicon diffusion might be expected. Also the decrease in activity between 400 and 600 Å would be expected to be similar to the increase between 600 and 800 Å; but at 800 Å considerable activity still remained. Furthermore silicon self diffusion in NiSi has been shown to be low[57] at the annealing temperature used (400 °C).

(iii) That the observed results are actually an artifact of the sputtering process must also be considered. In the

sputtering process the surface of the sample is bombarded with keV Ar^+ ions. After the initial primary collision the subsequent collision cascade imparts energy to a number of atoms, which become displaced from their original lattice positions. Considerable mixing at an interface is consequently to be expected. Poate et al[32] have concluded that 'one cannot probe an interface by sputter sectioning without seriously perturbing the very interface under investigation'. In this case mixing of Si and Si^* at the $NiSi^*$/NiSi interface would cause flattening of the measured profile integral, as was found. This seems to be the best explanation for the observed spreading, except that a similar effect might then have been expected in the Ni_2Si results, and this was not observed (Fig. 3.6).

It is concluded that the spreading may have been caused by thermal or sputter induced mixing of the Si and Si^*; further experimentation is required to determine the cause with more certainty.

Earlier ^{31}Si tracer work on NiSi by Botha was reproduced in Fig. 1.14. Although this earlier work did not show the same degree of profile spreading near the $NiSi^*$/NiSi interface as the current results, the overall results were similar, leading also to the conclusion that growth occurred by nickel diffusion. It is noted that in this earlier work only three data points, with large error bars, were obtained, so

the actual profile shape could not have been assigned with much certainty.

Current results are also in agreement with the work of Baglin et al[55], where NiSi growth was investigated using ^{56}Ni as the radioactive tracer. Their results showed considerable spreading of the Ni^* profile, as expected for high nickel mobility, but with the activity generally located in the expected region for NiSi formation by nickel diffusion. They were able to conclude that NiSi growth is dominated by substutional motion of nickel.

The results of the inert marker experiments on NiSi growth were given in Fig. 4.7-4.9. Both the Mo And Ta experiments showed marker movement consistent with nickel diffusion during second phase silicide growth. These results are in agreement with earlier work of this nature using X, Pt, and ^{16}O (Ref. 40, 41, and 42 respectively) as markers. Marker movement *proved* that NiSi growth occurred by dissociation of Ni_2Si :

$$Ni_2Si \rightarrow NiSi + Ni$$

The free nickel diffused through the layer of already formed NiSi above the marker, and through the marker, to subsequently form a second unit of NiSi. The results do not prove whether the second unit of NiSi formed immediately below the marker (following Si diffusion to this point), or at the Si/NiSi interface. However, given that the dissociation of Ni_2Si occurs, releasing nickel atoms, which

diffuse through the top half of the NiSi, it is reasonable to assume that these continue to move through the lower half of the NiSi to the Si/NiSi interface, to form more NiSi. This argument is supported by the experimental evidence of Botha et al[57] and Baglin et al[55] where respectively, silicon was found to have low mobility in NiSi, and nickel high mobility. It is noted however that the marker experiments, when considered in isolation, are not fully conclusive as it is possible that the reaction mechanism may have been forced by the presense of the marker layer. Reaction rate was found to be somewhat lower (~ ½) with , than without the marker.

In conclusion it is observed that the ^{31}Si tracer experiments on NiSi formation have shown that growth occurs by dissociation of NiSi :

$$Ni_2Si \rightarrow Ni + NiSi$$

This is in agreement with earlier work by Botha[31], and consistent with experimental observations that silicon has low mobility in (already formed) NiSi (Ref. 57), and nickel high mobility[55] during the growth of NiSi.

Some spreading of the Si^* activity profile was measured in the region near the expected $NiSi^*/NiSi$ interface. No ready explanation for this spreading could be found, but it is postulated that it may have been caused by mixing of Si and Si^* induced by the sputtering process.

Inert marker experiments using Ta and Mo as markers gave results consistent with nickel diffusion during growth, which is in agreement with published inert marker results.

CHAPTER 5

SUMMARY AND CONCLUSION

The growth of Ni_2Si from nickel and Si(a), and NiSi from Ni_2Si and Si(a), has been investigated by ^{31}Si radioactive tracer techniques, and by Kirkendal type inert marker experiments. In the tracer experiments samples were prepared with certain regions containing the radioactive ^{31}Si isotope; subsequent to annealing the location of the Si^* was determined by RF sputter microsectioning and activity counting. In the case of the inert marker experiments an ultra-thin (5-10 Å) metallic layer (Ta or Mo) was vacuum deposited within the sample prior to annealing. The position of the marker before and after silicide growth was determined by RBS spectroscopy.

The experimental results on Ni_2Si growth were described in chapter 3. The results of the Si^* tracer experiments (Fig. 3.6) showed, within experimental uncertainty, that after annealing the radioactive silicon was positioned within a surface layer of Ni_2Si, of concentration and thickness equivalent to that expected for nickel diffusion during silicide growth. This was further illustrated in Fig. 3.10, where the activity profile obtained by differentiating the straight line fit to the data of Fig. 3.6 produced the shown square profile, of ca. 100% activity concentration.

The Ni_2Si ^{31}Si tracer results in this investigation were different to that obtained by Pretorius et al[50] (Fig. 1.13), where the surface activity was shown to have dropped to about 60%, and considerable spreading was evident. Current results are consistent with previous work[31] on NiSi (and also with current NiSi results), whereas the previous Ni_2Si results apparently were not (Section 1.9); as investigation of this point was one of the primary objectives of this work it is worth considering how the disparity in results may have arisen. It is noted that some differences exist in the actual reactions investigated in the work of Pretorius et al, and in this work. In the previous work the reaction of nickel with crystalline silicon (Si<100>) was studied, i.e. virgin samples of structure Si<100>/Si^*/Ni were analysed. In this work the reaction between nickel and amorphous silicon was investigated, i.e. virgin samples of form Si<100>/Si(a)/Si^*/Ni. While it is not anticipated that there should be any significant differences in the diffusion mechanism or species for reaction of Ni with Si<100> or with Si(a), the original Ni_2Si^* results *may* have been influenced by the presence of the native oxide layer (Section 1.4) between the Si<100> and Si^*. For the reaction with Si<>, diffusion through this oxide layer must occur once the Ni_2Si^* layer has formed, whereas this is not so for the reaction with Si(a). It was observed in Section 1.4 that the presence of impurities can have profound effects on solid state reactions; it is not however clear at this stage if or

how the presence of such an impurity layer may have caused the drop in surface activity concentration and profile spreading observed by Pretorius et al[50].

The Ni_2Si Si^* tracer results unequivocally show that the reaction of nickel with amorphous silicon occurs by nickel diffusion, and bearing in mind the above discussion, the reaction with Si<> is expected to occur similarly. The diffusion mechanism could not be determined as Si^* tracer experiments are insensitive to metal (Ni) diffusion mechanism. The results are consistent with our subsequent measurements for NiSi formation, and also with the ^{56}Ni tracer work of Baglin et al[45].

In chapter 4 the results of the ^{31}Si tracer experiments on NiSi formation from Ni_2Si and Si(a) were presented. The results showed that during NiSi growth a surface layer of $NiSi^*$ formed; the activity concentration in this layer was found to be ~100% (where 100% was the calculated expected concentration for second phase nickel diffusion, and 50% that for silicon diffusion) for the first 400 Å approximately, with subsequent spreading of the radioactive silicon being observed. It is concluded that NiSi formation occurred by dissociation of Ni_2Si :-

$$Ni_2Si \rightarrow NiSi + Ni$$

The free Ni subsequently diffused through the already formed NiSi layer to form a second unit of NiSi at the Si(a)/NiSi interface. As was the case for the Ni_2Si^* experiments, the

mechanism of diffusion could not be determined. The spreading of the Si^* activity near the expected NiSi/$NiSi^*$ interface is not readily accounted for, but it is surmised that it may have been caused by sputter induced mixing of Si and Si^* at the interface.

The determination of nickel as the diffusing species during NiSi growth is in agreement with tracer studies by Botha[31] and Baglin et al[45], as well as with inert marker experimental results (Table 1.4). The $NiSi^*$ results are also consistent with the Ni_2Si^* results of this work.

The Si^* tracer experimental technique has been shown to be effective in the analysis of thin film solid state reactions. It was nevertheless pointed out in chapter 4 that the experimental precision is insufficient to permit the assignment of an exact shape to the activity profile by differentiation of the experimental data. To profile the radioactivity in a sample , over a depth of the order of 1000 Å, is not a trivial task, and uncertainties in results stem from a number of sources. The effects of activity counting statistics and RBS thickness determination have already been discussed and estimated. Irregularities in results which are less easily estimated are also however present, as a result of, for instance, sample differences, irregular interfaces, and particularly due to undesirable effects resulting from the sputter microsectioning of samples. During sputtering the sputtering particles deposit

energy in the sample, which can lead to changes in relative atomic composition or affect interfaces[32]. Further degrading effects such as laterally non-uniform sputtering, or preferential sputtering of metal or silicon could also occur. It is surmised that such sputtering effects may have occurred to some extent as the data obtained for the sputtering rates (Fig. 3.4 and 4.4) showed more scatter in the points than could be accounted for by the uncertainty in the RBS thickness determination. It is thus concluded that the experimental precision that can be obtained by the techniques used is relatively limited, and that within these limitations good quality results have been obtained in this work.

In the inert marker experiments a thin continuous layer of Mo or Ta was used as the marker. Marker movement was found to be consistent with nickel diffusion in both Ni_2Si and NiSi formation. These results are in complete agreement with previous inert marker experiments (Table 1.4). It is noted that these particular markers have not previously been used in the study of nickel silicide formation.

Evidence has been presented to convincingly establish nickel as the diffusing species in both Ni_2Si and NiSi formation. The question of why this should be so is yet to be given a definitive answer. For first phase formation, Tu et al[35] have proposed that the crystal structure of Ni_2Si favours the diffusion of nickel by allowing nickel vacancy diffusion

in both the nickel and silicon sub-lattices. It is noted however that the work of Baglin et al[55], using Ni^* as radioactive tracer, showed that Ni_2Si growth occurs partly by nickel substitutional diffusion, (i.e. ~ 50% Ni GB and 50% Ni substitutional diffusion), and their Ni^*_2Si profile showed the spreading expected from the high Ni mobility implied. High Ni mobility through the Si sub-lattice might be expected to cause some intermixing of Si and Si^* in a ^{31}Si tracer experiment; the Ni_2Si^* results in this work however showed no spreading of the activity profile at all, thus apparently contradicting the argument. Alternatively Tu et al[32] have suggested that phonon energies at the annealing temperatures used are insufficient to dissociate the covalent bonds in silicon, so that the silicon atoms remain in the substrate (or Si(a) layer) until the arrival of nickel atoms. A continuous supply of nickel atoms at the Si/silicide interface is then required to keep the reaction going, making nickel the diffusing species. The argument is supported by the observed general trend[9] that the metal is the dominant diffusing species in low temperature silicide formation, and silicon in high temperature formation (although exceptions do exist). It is clear that more work is required in this field of study to establish with certainty why nickel is the diffusing species in nickel silicide formation.

In final conclusion it may be stated that the ^{31}Si tracer experiments, and the inert marker experiments, performed in

this investigation have convincingly confirmed nickel as the diffusing species in Ni_2Si and NiSi formation from Ni and Si(a). The results are expected to apply also to silicide formation from Ni and crystalline silicon. The results are inherently consistent between phases, and are also in excellent agreement with previous published work on nickel silicide formation.

REFERENCES

1 *Inorganic Reactions and Methods*, ed. by J.J. Zuckerman, (Verlag Chemie, publishers of the German Chemical Society), to be published.

2 *VLSI Fabrication Principles*, Sarab K. Ghandi, J. Wiley & Sons, 1983.

3 *Integrated Circuits*, Texas Instruments Electronic Series, R.G. Hibberd, McGraw-Hill, 1969.

4 *Integrated Circuit Engineering*, A.B. Glaser and G.E. Subak-Sharpe, Addison-Wesley, 1979.

5 *Silicides For VLSI Applications*, S.P. Murarka, Academic Press Inc., 1983.

6 F. Mohammadi, Solid State Technology, (1981) 65.

7 *Large Scale Integration*, ed. by L. Altman, McGraw-Hill, 1976.

8 A. Magro-Campero, J. Appl. Phys., **53** (1982) 1224.

9 *VLSI Electronics: Microstructure Science*, Vol 6, Ch. 6, M.A. Nicolet and S.S. Lau, Academic Press Inc., 1983.

10 D.M. Scott and M.A. Nicolet, Nucl. Inst. and Methods, **182/183** (1981) 655.

11 *The Solid State Chemistry Of Co-Si and Ni-Si Binary Thin Film Systems*, H.A. Ras, PhD dissertation, Univ. of Stellenbosch, 1987.

12 *Metallurgical Thermochemistry*, 5th edition, O. Kubaschewski and C.B. Alcock, Pergamon Press, 1979.

13 E.P. Donovan, F. Spaepen, D. Turnbull, Appl. Phys. Lett., **42** (1983) 698.

14 *Constitution of Binary Alloys*, 2nd edition, M. Hansen and K. Anderko, McGraw-Hill, 1986.

15 R.M. Walser and R.W. Benè, Appl. Phys. Lett., **28** (1976) 624.

16 M. Ronay, Appl. Phys. Lett., **42** (1983) 577.

17 B.Y. Tsaur, S.S. Lau, J.W. Mayer, and M.A. Nicolet, Appl. Phys. Lett., **38** (1981) 922.

18 R. Pretorius, Mat. Res. Soc. Symp. Proc., **25** (1984) 15.

19 U. Göselle and K.N. Tu, J. Appl. Phys., **53** (1982) 3252.

20 K.N. Tu, G. Ottaviani, U. Göselle, and H. Föll, J. Appl. Phys., **54** (1983) 758.

21 D.M. Scott and M.A. Nicolet, Nucl. Inst. and Methods, **182/183** (1981) 655.

22 L. Wieluński, D.M. Scott, M.A. Nicolet, and H. von Seefeld, Appl. Phys. Lett., **38** (1981) 106.

23 *Diffusion in Solids*, P.G. Shewman, McGraw-Hill.

24 *Diffusion Kinetics for Atoms in Crystals*, J.R. Manning, D. van Nostrand Co. Inc., 1968.

25 *Diffusion In Solids, Liquids, Gases*, W. Jost, Academic Press Inc., 1952.

26 J.S. Kilkaldy, Can. J. Phys., **36** (1958) 917.

27 G.V. Kidson, J. of Nucl. Mat., **3** (1961) 21.

28 L. Boltzman, Ann. Physik, **53** (1894) 960.

29 C. Matano, Japan. Phys. **8** (1933) 109.

30 A. Smigelkas and E. Kirkendall, Trans. AIME **171** (1947) 130.

31 *Solid State Diffusion in Metal Silicides*, A.P. Botha, PhD Dissertation, Univ. of Stellenbosch, 1982.

32 *Thin Films - Interdiffusion and Reactions*, ed. by J.M. Poate, K.N. Tu, and J.W. Mayer, J. Wiley & Sons, 1978.

33 K.N. Tu, J. Appl. Phys., **48** (1977) 3379.

34 W.K. Chu, H. Kräutle, J.W. Mayer, H. Müller, M.A. Nicolet, and K.N. Tu, Appl. Phys. Lett., **25** (1974) 454.

35 K.N. Tu, W.K. Chu, and J.W. Mayer, Thin Solid Films, **25** (1975) 403.

36 W.K. Chu, S.S. Lau, J.W. Mayer, H. Müller, and K.N. Tu, Thin Solid Films, **25** (1975) 393.

37 K.N. Tu, Appl. Phys. Lett., **27** (1977) 3379.

38 L.S. Hung, E.F. Kennedy, C.J. Palmstrom, J.O. Olowolafe, J.W. Mayer, and H. Rhodes, Appl. Phys. Lett., **42** (1983) 8.

39 K. Affocter, X.A. Zhao, and M.A. Nicolet, J. Appl. Phys., **58** (1985) 3087.

40 T.G. Finstad, Phys. Stat. Sol. (a), **63** (1981) 223.

41 T.G. Finstad, J.W. Mayer, and M.A. Nicolet, Thin Solid Films, **51** (1978) 391.

42 D.M. Scott and M.A. Nicolet, Phys. Stat. Sol. (a), **66** (1981) 773.

43 F. d'Heurle, S. Petersson, L. Stolt, and B. Stritzker, J. Appl. Phys., **53** (1982) 5678.

44 C.D. Lien, M. Bartur, and M.A. Nicolet, Proc. Symp. on Thin Films and Interfaces II, Mat. Res. Soc., ed. by J.E.E. Baglin, D.R. Campbell, and W.K. Chu, Vol. **25** (1983) 51.

45 C.D. Lien, M.A. Nicolet, and S.S. Lau, Phys. Stat. Sol. (a), **81** (1984) 123.

46 M. Bartur and M.a. Nicolet, J. Appl. Phys., **54** (1983) 5404.

47 C.D. Lien, J. Appl. Phys., **57** (1985) 4554.

48 A. Martinez, D. Esteve, A. Guivarc'h, P. Auvray, P. Henoo, and G. Pelous, Solid State Electron, **23** (1980) 55.

49 R. Pretorius, Z.L. Liau, S.S. Lau, and M.A. Nicolet, Appl. Phys. Lett., **29** (1976) 598.

50 R. Pretorius, C.L. Ramiller, S.S. Lau, and M.A. Nicolet, Appl. Phys. Lett., **30** (1977) 501.

51 R. Pretorius, C.L. Ramiller, and M.A. Nicolet, Nucl. Inst. and Methods, **149** (1978) 629.

52 A.P. Botha and R. Pretorius, Thin Solid Films, **93** (1982) 127.

53 A.P. Botha, R. Pretorius, S. Kritzinger, Appl. Phys. Lett., **40** (1982) 412.

54 R. Pretorius, A.P. Botha, and J.C. Lombard, Thin Solid Films **79** (1981) 61.

55 J.E.E. Baglin, H.A. Atwater, D. Gupta, and F.M. d'Heurle, Mat. Res. Soc. Proc., Nov. 1981.

56 C.D. Lien and M.A. Nicolet, J. Appl. Phys., **55** (1984) 4187.

57 A.P. Botha, R. Pretorius, S. Kritzinger, Thin Solid Films, **141** (1986) 41.

58 C.D. Lien, M.A. Nicolet, and S.S. Lau, Phys. stat. Sol. (a), **81** (1984) 123.

59 *Backscattering Spectrometry*. Wei-Kan Chu, J.W. Mayer, and M.A. Nicolet, Academic Press Inc. 1978.

60 *Helium: Stopping Powers and Ranges in All Elemental Matter*. J.F. Zeigler, Pergamon Press Inc. 1977.